Journal of Power Sources 640 (2025) 236619

Contents lists available at ScienceDirect

Journal of Power Sources

journal homepage: www.elsevier.com/locate/jpowsour

Pressure evolution and gas solubility of Li-ion battery electrolytes during thermal abuse conditions

Florian Baakes [a,b], Roger Song [b], Thomas Bernet [b], Jorge Valenzuela García de León [a], George Jackson [b], Claire S. Adjiman [b], Amparo Galindo [b], Ulrike Krewer [a,*]

[a] Institute for Applied Materials - Electrochemical Technologies, Karlsruhe Institute of Technology, Adenauerring 20b, Karlsruhe, 76131, Germany
[b] Department of Chemical Engineering, Sargent Centre for Process Systems Engineering, Institute for Molecular Science and Engineering, Imperial College, South Kensington Campus, London, SW7 2AZ, United Kingdom

HIGHLIGHTS

- Pressure rise in Li-ion battery partially caused by solvent & gas composition.
- Optimisation potential in safety margin for gas volume in Li-ion batteries.
- Inert gases used during solvent storage and assembly should have low solubility.
- Linear carbonates advance safety due to high solubility CO_2.
- Influence of conductive salt on pressure evolution is negligible.

GRAPHICAL ABSTRACT

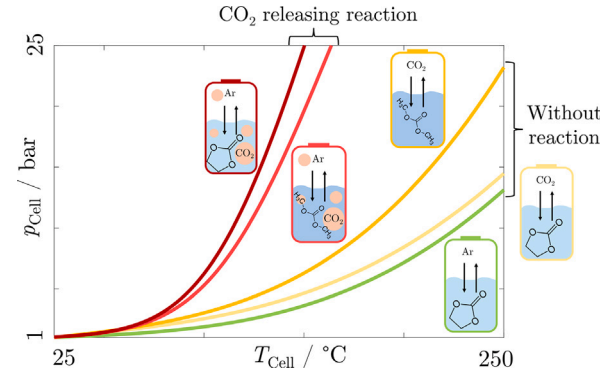

ARTICLE INFO

Dataset link: https://doi.org/10.35097/6j6r99kgrvjp09hs

Keywords:
SAFT-γ Mie
Linear/cyclic carbonates
Gas solubility
CO_2
Ar
$LiPF_6$
Vapour–liquid equilibrium

ABSTRACT

Understanding and controlling the evolution of pressure during thermal events of Li-ion batteries is a key aspect when assessing the safety of Li-ion batteries. In this study we evaluate the impact of solvent composition, gas solubility, and conductive salts on the pressure build-up during the exposure of the Li-ion battery electrolytes to high temperatures.

We employ a vapour–liquid equilibrium model based on the statistical associating fluid theory (SAFT)-γ Mie equation of state, extended to include an ion-pairing model to account for low degrees of salt dissociation in solvents with a low dielectric constant, such as linear carbonates. The effect of the degradation gases is accounted for by implementing a gas source mimicking a CO_2 evolving reaction.

We find that argon or nitrogen are good choices as inert gases during solvent storage and cell assembly, as they only gas out slightly during heating, i.e., they cause a negligible increase in pressure. Moreover, linear carbonates are found to be preferable over their cyclic counterparts regarding battery safety, as the higher solubility of degradation gases such as CO_2 in the electrolytes will mitigate pressure evolution during a thermal event. The presence of the conductive salt is found not to have a substantial effect on the pressure evolution.

The insights into the sensitivities of the pressure evolution presented here will allow to precisely tailor the composition of an electrolyte mixture to mitigate safety-critical gas evolution during a thermal event in Li-ion batteries.

* Corresponding author.
E-mail address: ulrike.krewer@kit.edu (U. Krewer).

https://doi.org/10.1016/j.jpowsour.2025.236619
Received 21 August 2024; Received in revised form 25 December 2024; Accepted 21 February 2025
Available online 21 March 2025

1. Introduction

The mass deployment of Li-ion batteries in electric vehicles, mobile applications, and stationary energy storage has led to an associated increase in the number of reported safety incidents [1,2]. Thermal runaway, a cascade of degradation exothermic reactions, drives these events. Most of these degradation reactions produce gases which lead to a build-up of pressure in the Li-ion cell [3,4]. This can result in the venting of the battery, ejecting toxic reaction gases, such as hydrogen fluoride, and flammable solvent molecules, and, in the worst case, an explosion of the battery [2]. Two key aspects are required to predict the evolution of pressure during the thermal abuse of Li-ion batteries: First, a reaction model that can be used to describe the amount of gases released from degradation reactions is paramount; Second, knowledge of the solubility of the evolving reaction gases in the liquid electrolyte must be known to calculate the pressure. In the current work we address the second challenge, having addressed the first in our previous studies [3,5].

We first give a brief literature review of existing studies on the impact of battery materials on pressure evolution. Golubkov et al. [6] measured the pressure during thermal runaway within an accelerating rate calorimetry (ARC) testing chamber using the ideal-gas law to calculate the total amount of ejected gases from a measure of pressure with increasing temperature. In their study, 18650 cells with three different cathode active materials, namely $LiFePO_4$ (LFP), $LiNi_{0.45}Mn_{0.45}Co_{0.10}O_2$ (NMC), and a blend of $LiCoO_2$ and $LiNi_{0.50}Mn_{0.25}Co_{0.25}O_2$ (LCO/NMC), were investigated. They found that the $LiCoO_2$/$LiNi_{0.50}Mn_{0.25}Co_{0.25}O_2$-blend released the highest amount of gases: 265 mmol after increasing the temperature from 25 °C to 850 °C. The pure NMC-type came second, releasing 149 mmol for the same temperature increase, and the LFP cell produced the least amount of gases releasing only 50 mmol. They also found that for the batteries investigated, the amount of gases released, with a corresponding increase in pressure, and the highest temperature reached during the ARC test were directly correlated. Lei et al. [7] used a similar technique to investigate Li-ion cells using $LiMnO_2$ as active material instead, and found that the amount of released gas, and thus the pressure increase, was 76.5 mmol, i.e., substantially lower than the reported values for NMC and LCO/NMC blends from [6]. Jhu et al. [8] studied four commercially available LCO cells at different states of charge, using a vent sizing package 2 (VSP2) adiabatic calorimeter, in which the overpressure in the cell is compensated by the testing chamber so that the Li-ion battery remains intact. They found that charged batteries are thermally more hazardous, with a pressure maximum which is up to 5.5 times higher than that of an uncharged cell. Significant differences in the pressure increase between the various LCO-type commercial cells was reported, indicating that other components, apart from the active material, also play a major role in the pressure evolution during thermal abuse of Li-ion batteries.

Even though the pressure of the testing chamber gives an insight into of the reactivity of active materials, no direct correlation to the internal pressure evolution before the venting of the cell can be drawn. Some authors have therefore incorporated a pressure sensor directly into the Li-ion cell [7,9]. However, as pointed out by Vendra et al. [10], such sensors are challenging to construct, and no two identical experiments are reported to yield comparable pressure curves.

Owing to the challenge of obtaining a pressure evolution from inside a Li-ion cell during thermal abuse, mathematical models are employed to aid in this matter. Coman et al. [9] used a combination of a representative gassing reaction and the vapour-pressure curve of dimethyl carbonate (DMC) as solvent to simulate the venting behaviour of a cylindrical 18650 cell to successfully reproduce the measured venting behaviour. Kim et al. [4] used a three-dimensional CFD simulation to investigate the venting behaviour of 18650 cells, with the calculations suggesting that most of the gases are produced during the rapid heating phase of the thermal runaway. Vendra et al. [10] measured the pressure in the ARC testing chamber and used the corresponding values of the pressure with an analytical equation to set initial conditions for their CFD simulation of fire dynamics. This review highlights that while significant progress has been made, existing research remains limited by the availability of experimental data, the constraints of current models, and the lack of investigations into pressure changes under varying working conditions, such as different charge/discharge rates and ambient temperatures.

The focus of the aforementioned studies is on the total pressure and gases produced (i.e., the venting behaviour) and on the cathode active material. It is known, however, that the so-called solid-electrolyte interphase (SEI), a protective surface layer that is formed in the initial formation cycles of a Li-ion battery, degrades at around 100 °C also releasing gases in the process [3,5,11]. Given the complexity of the reaction network governing the formation and degradation of the SEI [12,13] and the challenges in experimentally assessing its properties [14,15], there is a clear need for future development of a combined reaction and vapour–liquid equilibrium model. However, the current study focuses specifically on developing the vapour–liquid equilibrium model as a foundational step towards addressing this need.

To the best of our knowledge, a systematic analysis of the impact of the choice of solvent components, atmospheric and degradation gases, and the conductive salt, on the vapour–liquid equilibrium in Li-ion batteries has not been performed. One reason for this research gap is that liquid electrolytes are highly non-ideal systems. Conventional Li-ion battery electrolytes consist of a mixture of linear carbonates such as dimethyl carbonate (DMC), ethyl methyl carbonate (EMC), diethyl carbonate (DEC), and cyclic carbonates such as ethylene carbonate (EC) or propylene carbonate (PC), and conductive salt, most commonly $LiPF_6$ [16–18]. The number of mixtures of these components used in academia and industry is vast. Even though all consist of more or less the same molecules, their precise composition varies widely. Performing a systematic experimental analysis of their impact on thermal safety behaviour would therefore be a very time-consuming task. Additionally, the lack of reliable data of vapour–liquid equilibria of electrolyte solutions hinders the development of models. Quantitative models for the phase equilibria are nevertheless a prerequisite to predict the evolution of pressure. For classical cubic equations of state (EoS), experimental data for the precise system investigated is needed. Group contribution mixing rule extensions, such as the widely employed EoS/G_E, could, in theory, yield a predictive description [19]. However, polar substances, such as water or EC, are not well represented by classical EoS alone [20].

Advanced molecular-based methods such as the statistical associating fluid theory (SAFT) EoS developed in the late 1980s by Chapman et al. [21,22] can successfully aid in this matter. Stemming from the first-order thermodynamic perturbation theory of Wertheim [23–26], the SAFT approach can account for hydrogen-bonding interactions (association) and molecular non-sphericity. The approach has been shown to be accurate in the description of broad classes of fluids and mixtures with an accuracy surpassing classical cubic EoS [27,28]. The underlying approach has been adapted and developed further such that now a variety of SAFT theories exists, including the perturbed chain-SAFT [29,30], soft-SAFT [31], and SAFT-variable range [32]. The SAFT EoS has been further extended to incorporate a group contribution approach [33,34], based on the a Mie (generalised Lennard-Jones) potential [35], to describe the group interactions [36,37] as well as electrolyte solutions [38,39]. The resulting equation is known as the SAFT-γ Mie EoS [40].

In the original work extending the SAFT-γ Mie approach to electrolyte solutions [38] fully dissociated electrolyte systems were considered. This assumption is not appropriate for solvents with low dielectric constants [41]. A good example is DMC which has a dielectric constant of 3.13 at 25 °C [42], compared to 78.3 for water [43]. Even though the dielectric constants of EC and PC are 80 and 60 (at 25 °C), respectively, given the low dielectric constant of DMC, complete dissociation of $LiPF_6$ in electrolyte mixtures of DMC and EC or PC is not, therefore,

expected [41,44]. In the case of PC, the degree of dissociation of $LiPF_6$ is of the order of 70%–50% for concentrations from 0.5–2M, respectively [45]. From a modelling perspective, the undissociated salt also corresponds to a neutral ion pair [46] in solution; i.e., some dissolved ions form pairs bonded by non-directional electrostatic forces [46]. Ion-pair formation affects the amount of free ions and their interaction with the solvent molecules [47] and, as a consequence, the phase behaviour of the system. To account for this effect, in the current work we treat the salt dissociation by combining the SAFT-γ Mie model with an external calculation of the salts' dissociation formulated by Krienke et al. [48].

We employ the SAFT-γ Mie EoS to analyse the pressure evolution of conventional Li-ion battery electrolytes subjected to thermal abuse conditions. The necessary EoS parameters are estimated first and the resulting description is compared to suitable experimental data. An analysis of pressure evolution during heating to 250 °C is then addressed by investigating the influence of different solvent compositions. The effects of argon and CO_2 as storage gases for the electrolyte and the influence of the $LiPF_6$ concentration are also examined. A CO_2 source is then introduced to mimic the influence of gas evolution due to degradation reactions during thermal abuse, and its impact is investigated. We thus provide an in-depth understanding of the contribution of electrolyte solutions to the pressure evolution in Li-ion batteries before cell venting, which aids in exploring mitigation strategies.

2. Methods

In this section, an overview of the model and approximations underlying the SAFT-γ Mie approach are presented. The key considerations for the incorporation of ion pairing are also presented. This is followed by a brief description of the molecular models. Details of the assumptions required to model a Li-ion battery and the procedure for verification are then provided.

2.1. SAFT-γ Mie

In the SAFT-γ Mie approach [36,37] a heteronuclear model of fused spherical segments, which interact via Mie potentials of variable range, is employed. Short-range attractive sites are embedded in the spherical segments to mediate association interactions (e.g., hydrogen bonds). Molecules are modelled in terms of their constituent chemical groups: each group k is represented by a number v_k^* of identical spherical segments, and a molecule i contains v_{ik} groups of each type $k \in G$, the set of all groups in the mixtures. For example, DMC is modelled with one OCOO (linear carbonate group), and two CH_3 (methyl) groups (see Fig. 1). Additionally, each segment is characterised by a corresponding shape factor S_k, which describes the extent to which a given segment contributes to the total free energy. The interaction between segments k and l is modelled as a Mie potential:

$$\Phi_{kl}^{\mathrm{Mie}}(r_{kl}) = C_{kl}\varepsilon_{kl}\left(\left(\frac{\sigma_{kl}}{r_{kl}}\right)^{\lambda_{kl}^{\mathrm{r}}} - \left(\frac{\sigma_{kl}}{r_{kl}}\right)^{\lambda_{kl}^{\mathrm{a}}}\right), \tag{1}$$

where $\lambda_{kl}^{\mathrm{a}}$ and $\lambda_{kl}^{\mathrm{r}}$ describe the variable attractive and repulsive exponents, ε_{kl} is the depth of the potential well, r_{kl} represents the centre–centre distance between segments, and σ_{kl} is a size parameter which, for a like-like interaction, i.e. $k = l$ (σ_{kk}), is the segment diameter. Furthermore,

$$C_{kl} = \left(\frac{\lambda_{kl}^{\mathrm{r}}}{\lambda_{kl}^{\mathrm{r}} - \lambda_{kl}^{\mathrm{a}}}\right)\left(\frac{\lambda_{kl}^{\mathrm{r}}}{\lambda_{kl}^{\mathrm{a}}}\right)^{\frac{\lambda_{kl}^{\mathrm{a}}}{\lambda_{kl}^{\mathrm{r}} - \lambda_{kl}^{\mathrm{a}}}}, \tag{2}$$

is a prefactor that ensures that the minimum of the potential well is always $-\varepsilon_{kl}$, independently of the chosen $\lambda_{kl}^{\mathrm{a}}$ and $\lambda_{kl}^{\mathrm{r}}$.

To account for association-type interactions present in polar and hydrogen bonding substances a number $n_{a,k}$ of short-range association sites of type a can be added to a given group. Typical site types include electron donor and electron acceptor. A short-range square-well potential interaction is implemented such that an association site of type a on segment k interacts with another site of type b on segment l as

$$\Phi_{kl,ab}^{\mathrm{HB}}(r_{kl,ab}) = \begin{cases} -\varepsilon_{kl,ab}^{\mathrm{HB}} & \text{if} \quad r_{kl,ab} \le r_{kl,ab}^{\mathrm{c}} \\ 0 & \text{if} \quad r_{kl,ab} > r_{kl,ab}^{\mathrm{c}}, \end{cases} \tag{3}$$

where $r_{kl,ab}$ is the distance between the centres of sites a and b, $\varepsilon_{kl,ab}^{\mathrm{HB}}$ is the association energy, and $r_{kl,ab}^{\mathrm{c}}$ is the cut-off range of the interaction between the two sites, which can be equivalently described via a bonding volume $K_{kl,ab}^{\mathrm{HB}}$. To account for the contribution of interactions of ions with the uncharged (solvent) species, a Born term is considered. Here, the diameter of the Born cavity $\sigma_{kk}^{\mathrm{Born}}$ is introduced, which in the current work is also treated as an adjustable parameter.

The SAFT-γ Mie EoS is typically expressed in terms of the Helmholtz free energy A, obtained from the individual contributions as

$$A = A^{\mathrm{ideal}} + A^{\mathrm{monomer}} + A^{\mathrm{chain}} + A^{\mathrm{association}} + A^{\mathrm{Born}} + A^{\mathrm{ion}}, \tag{4}$$

where A^{ideal} denotes the free energy of an ideal gas of non interacting molecules, A^{monomer} represents the interaction of monomeric segments via Mie potentials, A^{chain} is the free energy contribution resulting from the formation of molecular chains from the combined Mie segments, and $A^{\mathrm{association}}$ is the free energy arising from short-range directional interactions. These first four terms account for the non-ionic contributions [36,37,49]. The influence of charged species is considered in the last two terms [38,39,50], which are formulated within a primitive-model framework in which the electrostatic character of the solvent is depicted as a uniform dielectric medium. The A^{Born} term accounts for the ion-solvent electrostatic interactions in accordance with the Born model [51], while The A^{ion} term accounts for the Coulombic ion-ion interactions, derived using the unrestricted mean spherical approximation (MSA) [52,53].

2.2. Ion-pairing

Ion-pairing is a phenomenon that has intrigued scientists for more than a century [46]. Its effect on transport properties, such as the ion diffusivity in Li-ion electrolyte mixtures, has been discussed widely [41,54–57]. Some experimental evidence suggests that a high level of ion-pairing results in the rapid deterioration of the conductive salt when exposed to water [58]. Several models have accounted for it [50,59–61], and all of these approaches lead to an acceptable representation of the specific system under study. Yet, only Olsen et al. [61] investigated non-aqueous systems. In our current work, an ion-pairing model is implemented to model solutions with EC, PC, DMC, EMC, and DEC as solvents within the SAFT-γ Mie framework with the mean spherical approximation of the primitive model for asymmetric ion sizes [38,39]. Given the case of monovalent ions M^+ and X^- the formation of an ion-pair MX can be described as

$$M^+ + X^- \overset{K_{\mathrm{A}}}{\rightleftharpoons} MX \tag{5}$$

The degree of dissociation α can be calculated as a function of the association constant K_{A} ($m^3\,mol^{-1}$) characteristic of the salt (and solvent), the concentration of the salt in solution C ($mol\,m^{-3}$), the mean ionic activity coefficient $\gamma_{\pm}'$, and the activity coefficient of the ion-pair (neutral salt) γ_0' (the $'$ refers to the solvent free particles in solution) as

$$\frac{1-\alpha}{\alpha^2} = \frac{CK_{\mathrm{A}}(\gamma_{\pm}')^2}{\gamma_0'}. \tag{6}$$

The model has been adapted from Krienke et al. [48] and is implemented in MATLAB [62]. A detailed description of the model is found in the ESI.

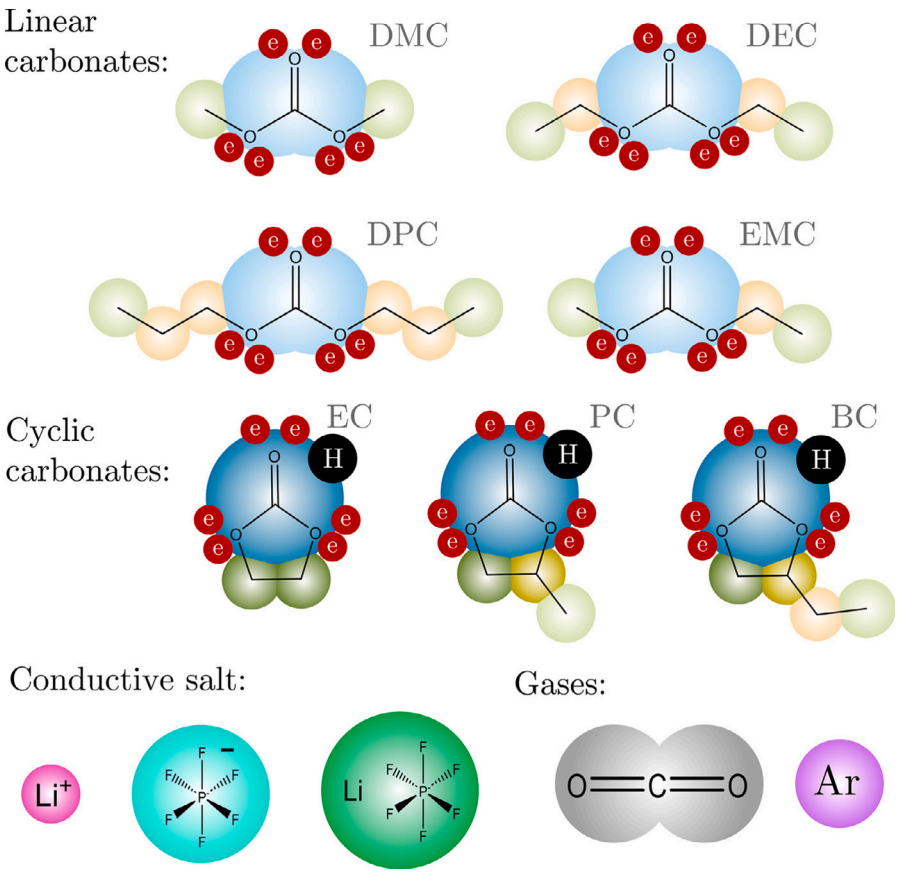

Fig. 1. SAFT-γ Mie representation of the molecules of interest in the current work. Linear carbonates, dimethyl carbonate (DMC), diethyl carbonate (DEC), dipropyl carbonate (DPC), and ethyl methyl carbonate (EMC); cyclic carbonates, ethylene carbonate (EC), propylene carbonate (PC), and butylene carbonate (BC); Li^+ and PF_6^-, and the ion pair $LiPF_6$; argon (Ar) and carbon dioxide (CO_2). Each coloured sphere or set of fused spheres of the same colour represent a different group in the model. The red and black circles marked with e and H refer to the electron donor and acceptor sites, respectively. (For interpretation of the references to colour in this figure legend, the reader is referred to the web version of this article.)

2.3. Molecular models

Each of the molecules considered in the current work is represented in Fig. 1 together with its corresponding SAFT-γ Mie model.

The linear carbonates, namely DMC, EMC, DEC, and dipropyl carbonate (DPC), incorporate the CH_3 group and a newly introduced linear carbonate OCOO group; additional CH_2 groups are introduced depending on length of the alkyl side-chains of each compound. The cyclic carbonates, EC, PC, and butylene carbonate (BC), include cCH_2 (where "c" denotes the CH_2 group appearing in a cycle), and a new cyclic carbonate group cOCOO. For PC and BC, which also contain a side-chain, the groups cCH, CH_2 and CH_3 need to be considered. Since $LiPF_6$ is the most commonly used conductive salt for state-of-the-art Li-ion batteries, the ions Li^+, PF_6^-, and the neutral ion-pair $LiPF_6$ are considered in the current work. In terms of gases, carbon dioxide (CO_2), one of the major degradation gases associated with thermal abuse of Li-ion batteries [6,63,64], and argon (Ar), the most frequently used inert gas in glove boxes of academia, are assessed.

In order to obtain the thermodynamic properties of the mixtures of interest, the like (e.g. OCOO–OCOO) and unlike (e.g. OCOO–CH_3) SAFT-γ Mie group parameters are determined by minimisation of a suitable objective function that quantifies the error between model predictions and experimental data. In terms of the determination of unlike group parameters, the scarcity of data often poses a challenge. When insufficient data are available, initial values of the unlike parameters can be obtained from the respective like interaction parameters using combining rules [35–37,65]. The experimental data used in the current work include single-phase liquid density [66–68], vapour pressure [69–74], enthalpy of vaporisation [69,73,74], and binary and multicomponent mixture data [75–83]. The estimation procedure, thermodynamic property, and phase equilibrium calculations are performed using the numerical solvers and the SAFT implementation of the commercial software package gPROMS® [84] as well as MATLAB [62]. Alternative open-source software packages which are available to reproduce our calculations are available from SGTPy [85] and Claperoyn.jl [86]. For brevity, an exhaustive description of the procedure used to obtain the parameters, the parameter values obtained, and a discussion of the results are given in the ESI.

In our current study, 26 like and unlike new group interactions are characterised using 623 experimental points. The percentage average absolute deviation (AAD%) over all points is found to be 5.10%. Based on prior experience, such a deviation is small enough to deliver a reliable model for the study of the phase equilibria and the resulting pressure for given temperature, volume, and electrolyte compositions in Li-ion batteries due to the heating of the electrolyte.

2.4. Cell model assumptions, initial value calculations, and testing procedure

Before analysing the thermodynamic behaviour of the electrolyte system during thermal abuse, the procedure to model the system at common conditions of Li-ion battery operation is described. The following assumptions are made:

- The system is closed.
- The cell casing is rigid, as in prismatic and round cells [87].

- Vapour–liquid equilibrium is always maintained, which emulates very slow heating of the cell.

To ensure comparable results with a real cell, we will use the volume of a commercial cell from our previous work, subtracting the volumes of the electrodes, separator, and current collector, as these components are not investigated in the current study. The total volume considered is therefore set as $V_{\text{cell}} = 1.55$ mL, see [3,5]. Unlike in our previous work, in which the pore space in the electrodes and separator were assumed to be fully liquid, a gas phase is introduced here. As a result, a given percentage ($\epsilon_{\text{liq}} = \frac{V_{\text{Liquid}}}{V_{\text{Gas}}+V_{\text{Liquid}}}$) of V_{cell} is taken by a liquid-electrolyte phase, and the rest is a (pad) gas phase that mimics the atmospheric conditions during cell assembly and storage. The exact proportion of liquid phase in commercial batteries is uncertain. We therefore analyse the impact of this liquid volume percentage in a sensitivity analysis as part of the current work.

In order to evaluate the phase equilibria a full set of initial conditions must be known. We define the initial point of each study at a temperature of $T = 25\,°\text{C}$, ambient pressure $p = 1.01$ bar, and the cell volume defined above as $V_{\text{cell}} = 1.55$ mL. The only unknown is $\boldsymbol{n}$, which is the vector describing the amount of moles of each component in the system. In order to obtain these, we first start with a guess of the initial moles $\boldsymbol{n}_0$ calculated as

$$\boldsymbol{n}_0 = \frac{V_{\text{cell}}\epsilon_{\text{liq}}\epsilon_{\text{liq},0}\boldsymbol{\varrho}_{\text{liq}}}{\boldsymbol{M}} + \frac{V_{\text{cell}}(1-\epsilon_{\text{liq}})\epsilon_{\text{vap},0}\boldsymbol{\varrho}_{\text{vap}}}{\boldsymbol{M}}, \tag{7}$$

with $\epsilon_{\text{liq},0}$ and $\epsilon_{\text{vap},0}$ referring to initial guesses for the volume fraction of each component in the liquid and vapour phases, respectively. It is important to note that for mixtures with more than one solvent, $\epsilon_{\text{liq},0}$ includes the liquid volume fractions that are used to describe these mixtures, such as, e.g., DMC/EC 50/50 vol-%. Liquid compounds are set to 0 in the vapour volume fraction guesses. The volatile compounds (Ar and CO_2) are set to 0 in the liquid and to 1 in the vapour volume fraction guesses, respectively. $\boldsymbol{\varrho}_{\text{liq}}(T,p)$ and $\boldsymbol{\varrho}_{\text{vap}}(T,p)$ are the liquid and vapour densities of each pure component, and $\boldsymbol{M}$ refers to the vector of molar masses of each component. Since this initial guess does not account for dissolved gases at equilibrium, the volume at equilibrium $V_0(T,p,\boldsymbol{n}_0)$ will be smaller than the cell volume. To correct this more molecules are added:

$$\boldsymbol{n} = \boldsymbol{n}_0 + \Delta\boldsymbol{n}, \tag{8}$$

where $\Delta\boldsymbol{n}$ is given as

$$\Delta\boldsymbol{n} = \frac{(V_{\text{cell}} - V_0(T,p,\boldsymbol{n}_0))\epsilon_{\text{vap},0}\boldsymbol{\varrho}_{\text{vap}}}{\boldsymbol{M}}. \tag{9}$$

This corresponds to adding more volatile compounds to fill up the missing volume. The reader is referred to the ESI for details of the corresponding procedure. After the moles at initial conditions of $T = 25\,°\text{C}$, ambient pressure $p = 1.01$ bar, and the cell volume $V_{\text{cell}} = 1.55$ mL are determined, the phase equilibrium calculations are performed for a range of temperatures between 25 °C and 250 °C. Depending on the system this might be constant volume calculations ($V_{\text{cell}} = 1.55$ mL), referring to closed cells, or constant pressure calculations ($p_{\text{cell}} = 1.01$ bar) referring to open cells. To ensure robust convergence and in order to check for phase stability Tp and TV-flash algorithms included in the gPROMS® software packages are employed to solve the phase equilibria.

2.4.1. Constant volume vs. constant pressure

In a previous publication [3], we investigated the effect of the evolving gases on the vapour–liquid equilibrium in Li-ion cells during thermal abuse. Gas evolution resulted in an increase in the pressure of the system, which in turn suppressed the evaporation of the liquid phase as the temperature increased. The SAFT-γ Mie model developed here is used to study the differences in calculations at constant pressure and constant volume to gain a more thorough understanding of the safety implications of Li-ion battery electrolytes at elevated temperatures. A model with constant volume corresponds to an electrolyte in battery cells with closed rigid cell casings. The constant pressure case corresponds to cell set-up where the volume of the vapour phase is allowed to expand and adjust to the external pressure such as in *in-operando* gas analysis setups [88]. An intermediate case is also investigated, where first a constant pressure calculation is performed until the 10-fold of the initial cell volume is reached. Thereafter, a constant volume calculation is considered; this corresponds to expandable pouch cell with flexible cell walls. The systems are studied considering phase change and the effect of possible (endothermic) heat of vaporisation. The latter is especially interesting as it may have a cooling effect during the self-heating of the battery.

The following description can help to get a qualitative understanding of the effect of the heat of vaporisation on the self-heating of a Li-ion battery. Assuming a constant heating rate, and a heat capacity of the cell, $C_{\text{p,bat}} = 9.43\ \text{J}\ °\text{C}^{-1}$, corresponding to a cylindrical 550 mAh cell [89], from our previous works [3,5], the heat introduced into the system to cause a temperature rise ΔT can be estimated as

$$Q_{\text{Heating}} = C_{\text{p,bat}}\,\Delta T. \tag{10}$$

The heat of vaporisation is calculated using the molar enthalpy of vaporisation, $\Delta\underline{H}_{\text{Vap},\sigma}(T,p,\boldsymbol{n})$, as

$$Q_{\text{Vap}} = \sum_{\sigma}^{|\Omega_{\text{Solv}}|} \Delta n''_{\sigma}\Delta\underline{H}_{\text{Vap},\sigma}(T,p,\boldsymbol{n}), \tag{11}$$

where $\Delta n''_{\sigma}$ is calculated as the differences of n''_{σ}, which is the number of moles of any given solvent σ in the vapour phase, of two equilibrium calculations. $|\Omega_{\text{Solv}}|$ is the set of all solvents in the mixture investigated. Since the enthalpy of vaporisation is evaluated at a given temperature T this comparison is only valid for very small increments in temperature, for which we choose $\Delta T = 0.01\,°\text{C}$.

The ratio of heats $\frac{Q_{\text{Vap}}}{Q_{\text{Heating}}}$ is used as a characteristic to rate the potential cooling effects through the vaporisation of solvent species. Given a constant heating rate this ratio allows one to assess how much additional heat would have to be introduced into the system to maintain the same heating rate, counteracting the endothermic effect of vaporisation.

2.4.2. Influence of gas evolving reactions

One key aspect of the pressure evolution during thermal abuse of Li-ion batteries is the influence of produced gases that arise from thermal degradation reactions. A complete reaction model, comprising of the degradation of the conductive salt, the solid electrolyte interface, its reformation and eventually the decomposition of the cathode active material as well as the combustion of the solvent molecules such as employed in our previous works [3,5] will blur the understanding of pressure evolution effects from the electrolyte itself. Further, it needs additional effort to be implemented within the SAFT-γ Mie framework due to the lack of interaction parameters for common degradation gases (e.g., CO, H_2, POF_3, PF_5). Consequently, as a starting point, we consider only a single, CO_2-evolving reaction to evaluate the basic impact which CO_2, the most produced gas during thermal decomposition, will have on the gas–liquid equilibrium and the pressure evolution. Here we choose a pseudo-reaction that represents the conversion of the reactive cyclic carbonate EC into a pseudo-solid product (which does not influence pressure) and CO_2: EC $\longrightarrow$ Solid + CO_2. This aims to mimic the reformation of the SEI after its primary decomposition. The actual reactions occurring in the cell are more complex, involving several evolving degradation gases [5], so that, the calculations should be seen as a first estimate of how reactions may impact the pressure in a Li-ion battery during thermal abuse.

For simplicity, the extent of reaction Δn is modelled via a Gaussian distribution function as a function of T because this emulates a chemical reaction to achieve the desired change in molar amounts of

EC and CO_2. In this way, the composition used as an input for the phase equilibrium calculations is altered over the range of temperatures of interest. The changes in total number of moles of EC and CO_2 are calculated as follows:

$$n_{EC}(T) = n_{EC}(T = 25\,°C) - \Delta n(T), \tag{12}$$

and

$$n_{CO_2}(T) = n_{CO_2}(T = 25\,°C) + \Delta n(T), \tag{13}$$

with

$$\Delta n(T) = \left(\frac{\kappa}{2}\right)\left(1 + \mathrm{erf}\left(\frac{(T-\theta)}{\omega\sqrt{2}}\right)\right). \tag{14}$$

In Eq. (14), κ represents the total quantity of EC converted to CO_2, θ is the mean value of the distribution, which in this case refers to the temperature where the reaction rate exhibits its peak (set to 140 °C), such that the reaction is assumed to occur in the early phases of self-heating. This also ensures that the majority of the reaction is completed at $T = 200\,°C$, until which point most of the EC is still in liquid form, rendering this effectively a liquid-phase reaction. ω corresponds to the standard deviation of the distribution shaping the pseudo-reaction and has been set to 0.1θ.

3. Results and discussion

For understanding the gas–liquid phase behaviour in the electrolyte during thermal abuse, we consider two scenarios: one where the reactions due to electrolyte degradation are neglected, and another where a gas source simulating the conversion of EC into a solid and CO_2 is included.

3.1. Scenario omitting gas-evolving reaction

In the following, we analyse the impact of cell properties such as the liquid-to-void volume ratio, solvent composition, choice of pad-gas, constant pressure vs. constant volume, and the presence of the conductive salt $LiPF_6$, but neglect the impact of degradation reactions. By excluding reactions from the model, we can focus solely on the importance of the thermodynamic properties of the system for cell safety. This gives an appropriate baseline for later adding reactivity.

3.1.1. Impact of liquid volume percentage

Given that one of the primary design goals for Li-ion batteries is to maximise volumetric energy density, one may anticipate that the amount of gas phase within these batteries should be minimised to reduce the total cell volume and boost the energy density. However, Kupper et al. [90] and Coman et al. [9] estimated the liquid volume percentage as 70 and 50 vol-% from imaging data. Commercial Li-ion cells therefore have such a considerably large safety buffer that there might still be room for optimisation. Therefore, we first begin investigating the effect of different values of vol-% on the pressure evolution in Li-ion cells.

In Fig. 2 (a), the dependence of pressure on cell temperature for cells with a DMC/EC 50/50 vol-% mixture, with argon as pad gas, at initial liquid vol-% of 98, 95, 90, and 85 (at 25 °C) is presented. If not stated otherwise, argon is used as the pad gas, and the initial mixture composition is always given in volume percentages. Safety measures typically included in commercial batteries are the current-interruption device (CID) and a safety valve. The first, typically activating at 10 bar [91], is the CID. When activated, it disrupts the connection between the pole and the current collector, halting further current flow, thus reducing electrochemical reactions. The second, typically activating around 20 bar [91], is a safety valve that opens to release gases so that the pressure is reduced to safe levels.

In our model, a cell that is optimised for maximum volumetric energy density, with 98 vol-% of liquid phase would activate the safety valve at just 87 °C, even without including any side reactions. This phenomenon can be traced back to the effect of temperature on the liquid volume in the cell. At lower temperatures, where $\epsilon_{liq} < 1$, the liquid volume expands into the gas phase. This leads to a very small increase in the pressure. At the point where $V_{cell} = V_{liq}$ (subsequently referred to as volume parity), all of the light components are in the liquid phase. Any further increase in temperature would require the liquid to expand further but it is hindered by the cell wall, thus, the pressure increases. Since liquids are known to be largely incompressible, this results in the build-up of extreme pressures. The pressure massively increases from just under 2 bar to around 100 bar within a 5 °C change.

The lower the initial liquid vol-% the higher the temperature at which the sharp increase in pressure is observed, as the additional (gas) volume in the cell allows for expansion of the liquid over a larger temperature range. For the case with 85 vol-% initial liquid volume, volume parity is reached at 235 °C, and the sharp pressure increase with temperature is virtually not apparent from Fig. 2(a). These findings confirm that batteries should maintain a minimum free volume as a safety buffer to avoid explosion or venting at temperatures below 100 °C, which could be reached, e.g., due to fast charging. However, compared to the 70 vol-% [90] and 50 vol-% [9] initial liquid volume obtained from imaging data of commercial cells, the findings presented here suggest that the liquid volume percentage could be increased to 85 vol-% without risk of early venting below 200 °C due to liquid volume expansion, albeit under the assumption of slow heating. In Section 3.2, these calculations are revisited and extended to account for gases evolving from degradation reactions. To exclude the effect of sharp pressure increases due to volume parity at higher temperatures from further analysis, the initial liquid vol-% is set to 70 vol-% for all further cases. This corresponds to the void volume reported by Kupper et al. [90].

3.1.2. Impact of solvent composition

In Fig. 2 (b), a comparison between commonly applied solvent compositions is performed. The cases investigated include DMC/EC with 70/30 and 50/50 vol-%, and EMC/EC 70/30 vol-%. Additionally, a ternary mixture of DMC/EMC/EC 33/33/33 vol-% is investigated. We find that the solvent composition has no significant impact on pressure evolution at temperatures below 50 °C. Above this temperature, the curves are seen to deviate: the DMC/EC 70/30 vol-% mixture experiences the most significant pressure increase, and the EMC/EC 70/30 vol-% mixture the least. The other compositions lie in between these two. The DMC/EC 70/30 vol-% mixture reaches the activation pressure of the CID (10 bar) at 190 °C, while the higher boiling EMC/EC 70/30 vol-% mixture reaches it at 210 °C. The DMC/EC 70/30 vol-% mixture is the only one that reaches the safety valve opening pressure of 20 bar within the investigated temperature range, at 240 °C. DMC/EC mixtures with a higher EC content, e.g. DMC/EC 50/50 vol-%, exhibit a lower pressure over the whole temperature range. The DMC/EMC/EC 33/33/33 vol-% mixture presents an almost identical pressure evolution as the DMC/EC 50/50 vol-% mixture. This behaviour can be explained by the different boiling points of DMC (108 °C), EMC (115 °C), and EC (240 °C). For the investigated solvent compositions, the solvent choice can make a difference of up to 40% in pressure evolution. The deviations between the pressure evolution for all of the cases presented in our work are provided in the ESI.

Based on this analysis of Li-ion battery electrolyte under high-temperature abuse, we conclude that it is advisable to minimise linear carbonates in the electrolyte mixture. Higher boiling solvent alternatives, e.g., EMC rather than DMC, seem to be advisable when battery performance and costs permit. However, as will be discussed in Section 3.2, this is not generally true when considering gassing degradation reactions.

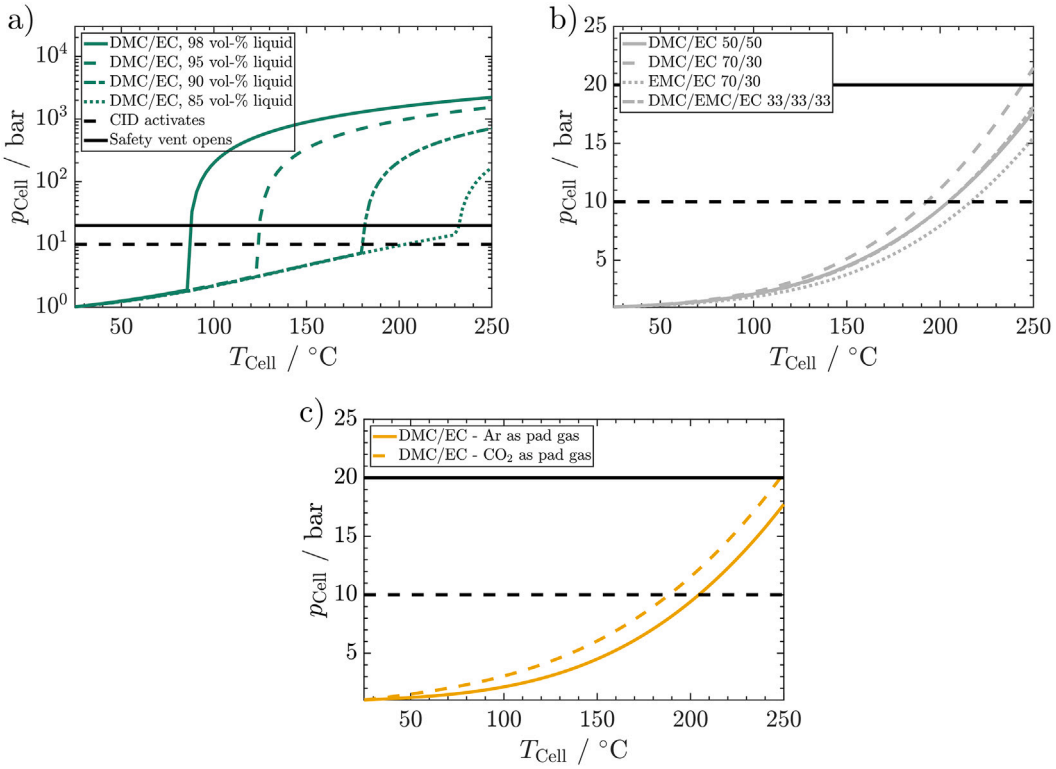

Fig. 2. Pressure evolution for a cell with different initial gas and electrolyte composition heated from T = 25 °C to 250 °C with a sufficiently slow heating rate to establish equilibrium: (a) The initial liquid-volume percentage is studied for DMC/EC 50/50 vol-% with argon as pad gas; (b) various global solvent compositions with argon as pad gas; (c) type of pad gas is studied for DMC/EC 50/50 vol-%. For the calculations in (b) and (c), the initial liquid vol-% is set to 70 vol-% to avoid reaching volume parity at lower temperatures. Safety measures are indicated as horizontal lines, CID by dashed, and safety vent by continuous black. (For interpretation of the references to colour in this figure legend, the reader is referred to the web version of this article.)

3.1.3. Impact of pad gas

We now compare two pad gases, CO_2 and Ar, using a DMC/EC 50/50 vol-% mixture. Ar is chosen as a pad gas because it is a common gas used to obtain an inert atmosphere for cell assembly in academic settings. CO_2 is chosen because it is reported, together with CO and H_2, as being present in the highest concentrations after a thermal runaway [6,63,64]. It is also useful to mention that argon has a 96% lower solubility in the given mixture at 25 °C and 1.01 bar than CO_2 (as calculated using the SAFT-γ Mie model developed here). The choice of these two gases thus provides a relevant comparison of how using different inert gases during assembly and storage impacts the pressure evolution, and thus safety, in Li-ion cells.

The mixture containing CO_2 as pad gas (see Fig. 2(c)) leads to up to 20% higher pressure compared to Ar. This may seem surprising as CO_2 has a higher solubility, which should lead to fewer molecules in the gas phase and, thus, a lower pressure. The higher pressure found for CO_2 is due to the storage and assembly conditions. In these procedures, gas is added to a given volume of solvent mixture until the cell volume is reached. This means that in the case of a compound with higher solubility, more gas molecules are present in the mixture at 25 °C, when the cell is assembled. As the temperature is increased, the CO_2 solubility in the liquid decreases, and more molecules are found in the gas phase, with a corresponding increase in pressure.

The calculations serve to identify two key properties for improved pad gases: the first is a low solubility of the pad gas in the liquid phase to reduce the number of light component molecules in the system; the second is endothermic dissolution such that the solubility of the gas rises with increasing temperature. Argon is found to exhibit both properties, with a enthalpy of dissolution in DMC of $\Delta \underline{H}_{\mathrm{Diss,\,Ar/DMC}} = 7.6\,\mathrm{kJ\,mol^{-1}}$ [79] compared to $\Delta \underline{H}_{\mathrm{Diss,\,CO_2/DMC}} = -16.85\,\mathrm{kJ\,mol^{-1}}$ [77]. However, as it is a noble gas that must be produced with a significant effort, it might not be economically feasible as an inert gas during solvent storage or cell assembly, especially on an industrial scale. Nitrogen is 38% less soluble in linear carbonates [92] than argon at room temperature, and may hence be a better choice for use on an industrial scale, as e.g., shown by [93]. Yet, it is known to react with Li metal [14]; whether it also reacts at high temperatures with a lithiated carbon electrode is an open question. This adds complexity to the safety assessment in this context and could be addressed in future studies.

3.1.4. Constant volume vs. constant pressure

We now explore the difference of considering constant volume vs. constant pressure systems in terms of changes in vapour volume fraction and resulting heat of vaporisation. Our previous study [3] suggested that due to evolving gases and, thus, increased pressure in a closed battery (expandable) cell, solvent boiling is suppressed until thermal runaway is reached. With the advanced phase equilibrium model of our current work, we are able to examine the pressure and volume dependencies in more detail.

A mixture of DMC/EC, 70/30 vol-% with argon as pad gas is investigated under constant volume (constant $V_{\mathrm{cell}} = 1.55\,\mathrm{mL}$), i.e., resembling a closed battery cell, and compared with constant pressure calculations (constant $p_{\mathrm{cell}} = 1.01\,\mathrm{bar}$), which resembles the behaviour of an open battery cell. A system that can expand to a maximum of 10 times the initial electrolyte volume (constant $p_{\mathrm{cell}} = 1.01\,\mathrm{bar}$ until $V_{\mathrm{cell}} = 10V_{\mathrm{cell,0}}$ then constant $V_{\mathrm{cell}} = 15.5\,\mathrm{mL}$) is also investigated. The latter case resembles a pouch cell that does not have rigid cell walls in contrast to prismatic and round cells.

In Fig. 3(a) the ratio of moles in the gas phase with respect to the total number of moles in the cell as a function of temperature is shown, expressed as a percentage in the three systems. For the case of constant volume calculations, only a small amount of matter transfer from the liquid to the vapour phase is observed; the percentage of the vapour phase does not exceed 1%. It can be concluded that

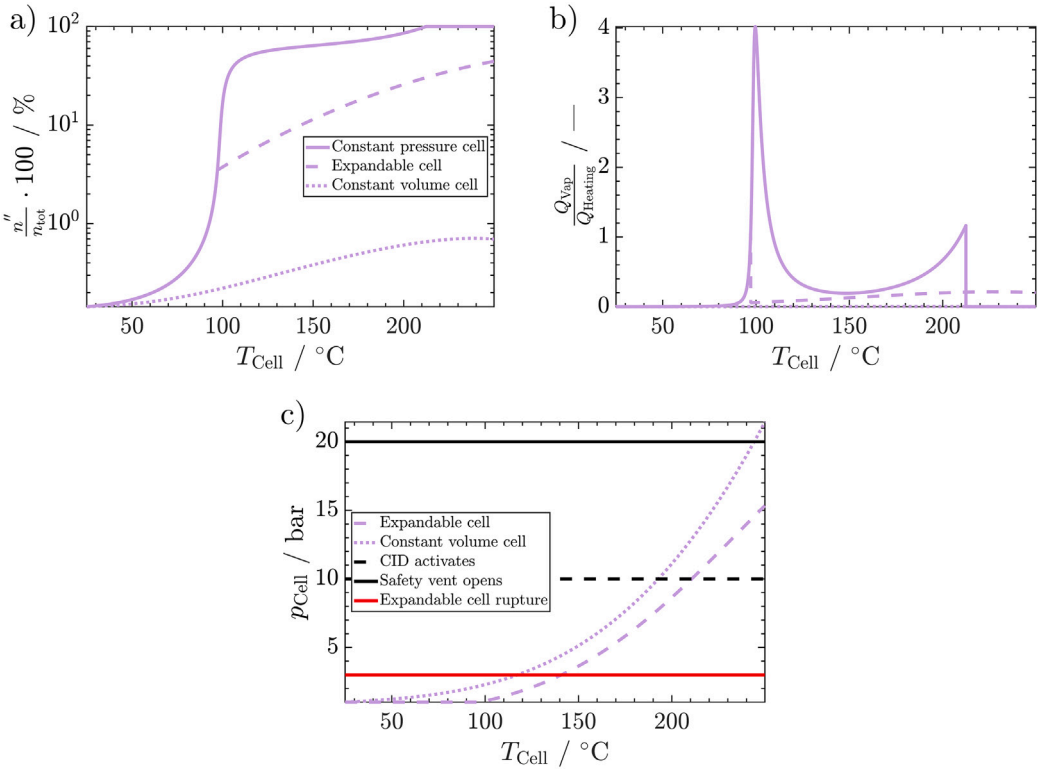

Fig. 3. Difference between the behaviour of constant volume cells (constant V_{cell} = 1.55 mL), expandable (constant p_{cell} = 1.01 bar until $V_{cell} = 10V_{cell,0}$ then constant V_{cell} = 15.5 mL), and constant pressure (constant p_{cell} = 1.01 bar) electrolyte systems in a cell heated slowly to 250 °C for a DMC/EC 70/30 vol-% mixture with argon as a pad gas. Effect on (a) vapour-phase percentage on a molar basis, (b) ratio of heat of vaporisation to heat needed for heating the cell at a constant rate, and (c) the pressure evolution for the closed and expandable cells. The initial liquid vol-% is set to 70 vol-%. Safety pressures are indicated as horizontal lines.

almost no solvent evaporation occurs over the investigated temperature range for a closed battery cell. It also follows that the cooling effect due to vaporisation in a closed cell will be almost negligible, which confirms the findings of our previous studies. The ratio of the energy of vaporisation to the energy introduced into the system to obtain a desired temperature in this cell is shown in Fig. 3(b). As can be seen the ratio is close to 0 over the whole temperature range, i.e., no cooling effect due to solvent boiling occurs. In contrast to the results from our previous study [3], the current analysis leads to the suggestion that no degradation reactions are needed to suppress solvent boiling, as none are considered in this case.

In the case of the constant pressure cell (constant p_{cell} = 1.01 bar) a first steep increase in vapour percentage from 80–100 °C is seen, followed by a second less steep increase from 150–200 °C. A 100% vapour fraction is reached at around 210 °C. These changes in slopes are related to the boiling temperatures of the linear carbonate (around 100 °C) and cyclic carbonate (around 200 °C), respectively. As expected, in a constant pressure cell, solvent boiling occurs close to the boiling point of the lower boiling linear carbonate and continues until all of the solvents have changed phase. The ratio between the energy of vaporisation and energy needed to heat the system (Fig. 3(b)) is seen to sharply increase around 90 °C and reaches a maximum of 4 at 100 °C, corresponding mostly to the evaporation of the linear carbonate. This ratio then decreases to reach a (local) minimum of 0.2 at 150 °C, as most of the linear carbonate is in the vapour phase. Thereafter, it rises again to reach a ratio of 1.1 at 210 °C, corresponding to the increased phase change of the cyclic carbonates. At higher temperatures, the ratio drops to 0 since 100% vapour phase fraction is reached and no further boiling can occur. It follows from these calculations that solvent boiling would severely influence the temperature progression in an open cell. Especially since the ratio first peaks around 100–120 °C, where the cooling effect is opposed by a relatively small amount of heat produced from exothermic reactions, as can been seen from our previous work [3,5].

The intermediate, expandable case exhibits the same behaviour as the constant pressure cell up to 97 °C when the maximum cell volume is reached. At this point, a vapour phase fraction of around 4% is obtained, which steadily increases to around 40% at 250 °C. The ratio between the energy of vaporisation and the energy needed to heat the system drops from 0.2 to almost 0 after reaching the maximum volume. However, with a further increase in temperature, it increases to 0.1 again. Based on these insights, it can be expected that contrary to cells with rigid walls, a liquid–vapour phase transition might occur in pouch cells during the thermal abuse of Li-ion batteries. This could beneficially influence the temperature gradient due to the associated cooling effect of the phase transition. Another important aspect to consider is that pouch cells will rupture at lower pressures than those used for the safety measures of cells with rigid cell walls, i.e., 3 bar [94], see Fig. 3(c). This speaks against improved safety of pouch cells as, even considering the more rapid temperature gradient in cells with rigid casings, this pressure is reached at lower temperatures than pressure of safety measures in the rigid casings, 10 bar and 20 bar for CID and safety vent, respectively.

3.1.5. Impact of conductive salt

We investigate the influence of the conductive salt $LiPF_6$ on the pressure evolution during heating for a closed cell. The chosen solvent system is a DMC/EC 50/50 vol-% mixture with CO_2 as pad gas.[1]

[1] In this case, CO_2 is used as a pad gas instead of argon since, due to numerical problems, the systems could not be solved using argon. We do not, however, expect significant differences in the impact of $LiPF_6$ when using Ar.

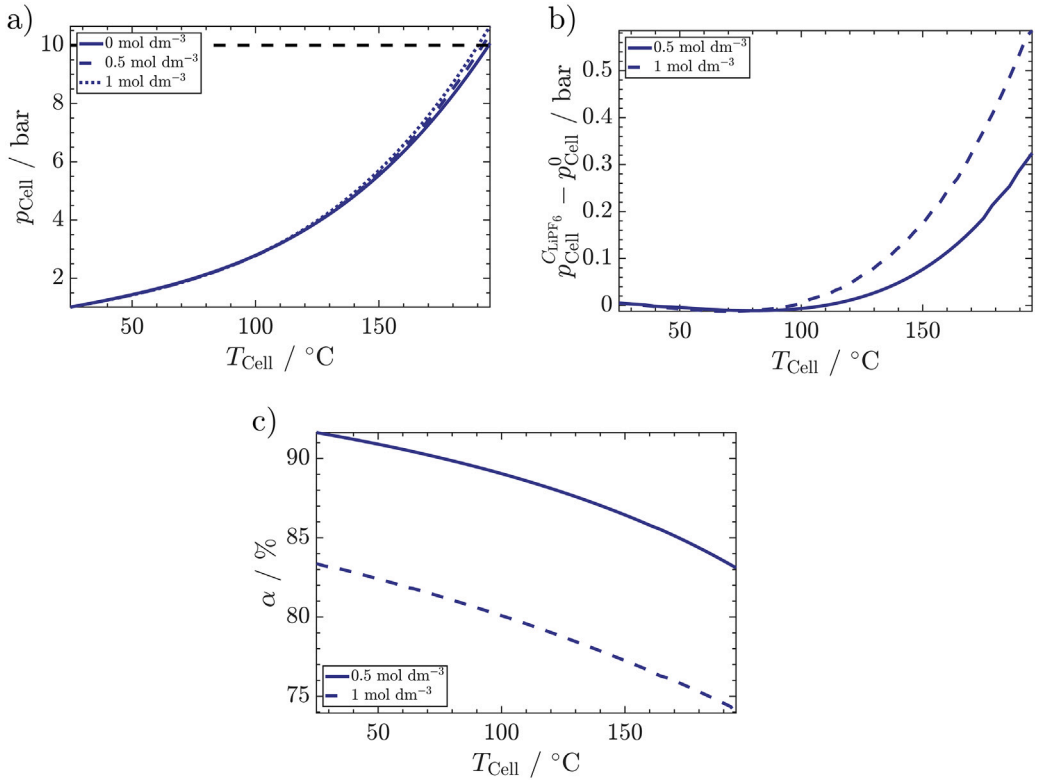

Fig. 4. Effect of $LiPF_6$ concentration on the behaviour of a cell heated to 195 °C with a DMC/EC 50/50 ol-% mixture with CO_2 as pad gas and 70 vol-% initial liquid volume. Impact on (a) pressure; (b) difference in pressure between the case with no salt and cases with added salt; (c) degree of dissociation.

In Fig. 4(a), the evolution of the pressure over the temperature range studied is shown for salt concentrations ranging from 0 to 1 mol dm^{-3}. As can be seen, the overall effect of the presence of salt is relatively small, with a maximum relative pressure deviation of 5% between 0 mol dm^{-3} and 1 mol dm^{-3}. The influence of $LiPF_6$ as the conductive salt is significantly smaller than that of other factors studied (e.g., solvent composition or pad gases). For a clearer picture of pressure progressions we show the pressure difference between the 0 mol dm^{-3} case and the cases including salt in Fig. 4(b). We should note that the graph here is only shown to 195 °C, since after this point liquid–liquid phase separation occurs, which we deem an artefact of the model as to the best of our knowledge this behaviour has not been observed experimentally. The same behaviour occurs for salt concentrations of 1.5 mol dm^{-3} already at 25 °C. However, as this has also not been reported for experimentally studied mixtures [95,96], it also appears to be an artefact. Therefore, these calculations are omitted from the presentation.

The reason for the pressure increase due to introducing salt into the system warrants further exploration. An inspection of literature data suggests that introducing $LiPF_6$ into pure DMC increases its vapour pressure [80], which indicates weak unlike interactions between $LiPF_6$ and DMC. Even though this contradicts the generally recognised trend that introducing salt into a liquid mixture will result in a lowering of vapour pressure (and elevation of boiling temperature) the experiments serve to confirm the validity of our thermodynamic model.

A further intriguing effect that can be investigated with our model is the degree of salt dissociation during thermal abuse. In Fig. 4(c) the degree of dissociation of the salt is shown. As can be seen, it decreases with increasing temperature and salt concentration. Both effects are similar in magnitude (±10% change) over the investigated range of concentrations and temperatures. This can be explained by the fact that apart from the salt concentration, the degree of dissociation is mainly influenced by the dielectric constant of the solvent. As shown in the ESI, the dielectric constant of high dielectric solvents such as EC decreases rapidly with increasing temperature, from 96 at 25 °C to 40 at 200 °C. This explains the lower degree of dissociation observed at higher temperatures. In operational environments of the battery, the conductive salt would start to degrade around 80 °C [5], such that, the total salt concentration in the electrolyte would be lower at higher temperatures.

In conclusion, the salt concentration seems to have no substantial effect on the pressure evolution within the boundaries of conventional concentrations around 1 M. This suggests that, based on our current knowledge, there is no trade-off between safety and performance when it comes to the conductive salt concentration, which allows for possible performance maximisation.

3.2. Scenario with a gas-evolving reaction

CO_2 producing reactions occur in the temperature range up to 250 °C [5]. We now consider the principle effect which gases originating from degradation reactions might have on the evolution of pressure and vapour–liquid equilibria in Li-ion battery electrolytes during a thermal event. The example gas used is CO_2. Alongside with H_2 and CO, CO_2 is the most measured degradation gas produced in a thermal event of a Li-ion battery [6,63,64]. We assume CO_2 to be released following a Gaussian curve shape, i.e., with an increase and then a decrease with temperature (see Section 2.4). The total amount of CO_2 released is chosen to reflect a conversion of 10, 15, and 20 mol-% of EC in the mixture, respectively. According to results of our previous publication [5], the conversions of different percentages of EC correspond to anodes with different thicknesses of the solid-electrolyte interphase (SEI). For a thick SEI, 10 mol-% EC were reported to react during the thermal event up to 250 °C. Anodes with a thin SEI, which were more reactive, showed a decomposition of 20 mol-% EC. Please

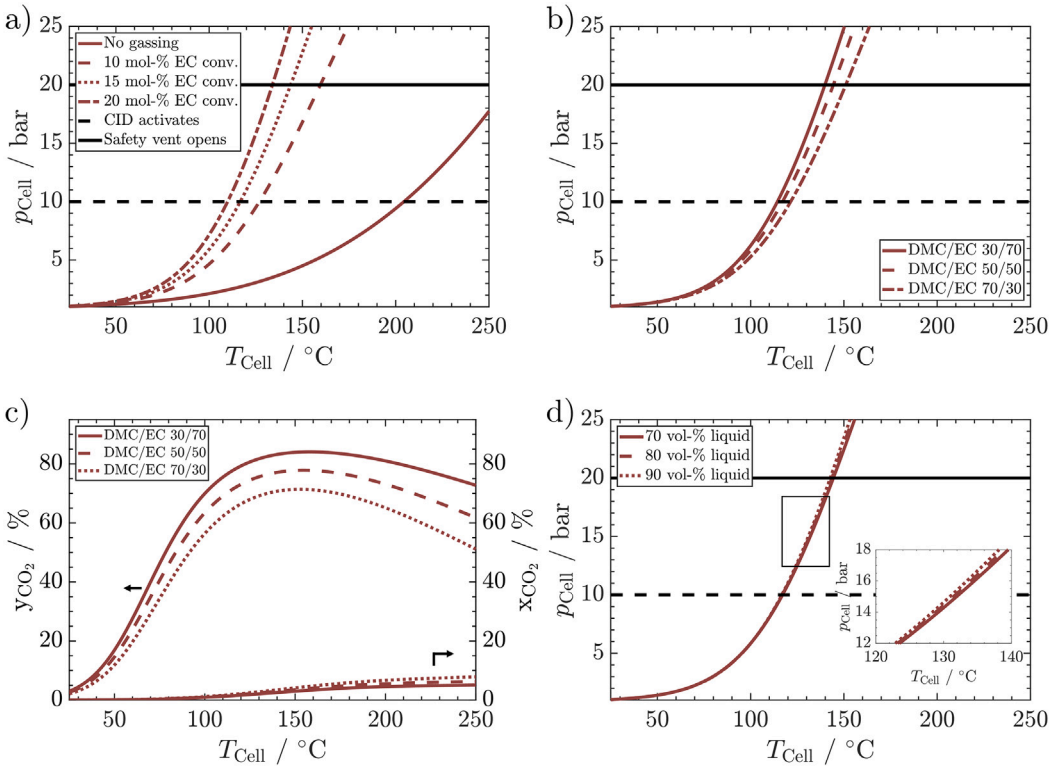

Fig. 5. Influence of a CO_2-evolving reaction during cell heating as a function of temperature (a) pressure evolution for varying extents of CO_2 released in mol-% of EC for a DMC/EC 50/50 vol-% mixture using argon as pad gas; (b) pressure evolution with varying initial solvent compositions with a fixed extent of released CO_2 corresponding to 15 mol-% EC in a 50/50 vol-% DMC/EC mixture); (c) CO_2 mole percentage in the gas and liquid phases for varying electrolyte composition. The initial liquid vol-% is set to 70 vol-% for all cases in (a)-(c); (d) pressure evolution with varying levels of initial liquid volume fraction for an extent of conversion of 15-mol-% of EC to CO_2 in a DMC/EC 50/50 vol-% mixture with 70 vol-% liquid volume system.

note that the analysis in the current work should only be considered as a first step in assessing reaction impacts on the pressure evolution. To gain a more accurate insight into the complex interdependency of gassing reactions, phase equilibria, and pressure evolution, a detailed analysis including a complete set of degradation reactions and a wider variety of evolving gases with their respective solubilities, needs to be considered in the future.

In Fig. 5(a), the results for a scenario with CO_2-evolving reaction with three different CO_2 amounts are shown for a closed cell (constant V_{cell} = 1.55 mL) with a DMC/EC 50/50 vol-% mixture using argon as pad gas. These calculations are compared with those for the system without CO_2-evolving reaction. As can be seen in the figure, the evolving gas tremendously amplifies the evolution of pressure with increasing temperature. The maximum deviation compared to the case with no CO_2-evolving reaction is 200% for the 10 mol-% EC conversion and further increases to 500% in the 20 mol-% EC conversion case. For all CO_2 amounts released, the cell reaches the CID activation in the range from 105 °C to 125 °C. Furthermore, the safety valve will open in all cases over the temperature range from 142 °C to 175 °C. This is in the reported temperature range of venting in ARC experiments [7,97].

In Fig. 5(b) we analyse the impact of solvent compositions in combination with a gas source mimicking a gas-releasing reaction. This is achieved by fixing the amount of EC converting to CO_2 to an absolute value of 15 mol-% of EC in a DMC/EC 50/50 vol-% mixture, independent of solvent composition. This analysis aims to provide a qualitative understanding of the impacts of different compositions on pressure evolution based on the change in gas solubility.

The highest pressure can be observed for the DMC/EC 30/70 vol-% mixture. The system reaches the safety valve pressure at 140 °C. The DMC/EC 50/50 vol-% mixture exhibits a slightly lower pressure evolution, with a maximum deviation for the DMC/EC 30/70 vol-% case of up to 10%. The lowest pressure in the investigated temperature range is observed for the DMC/EC 70/30 vol-% mixture. Interestingly, higher amounts of low-boiling linear carbonate DMC do not lead to higher pressures. This contrasts with our findings for non-reactive systems, where increasing amounts of low-boiling linear carbonates led to an increased pressure (see Section 3.1.2). This result suggests that a deeper look into the underlying processes is needed.

In Fig. 5(c), the corresponding CO_2 fractions in the vapour phase and liquid phase are shown. The vapour mole fraction of CO_2 exhibits a steep increase around 50 °C for all cases. It peaks between 140 °C and 150 °C depending on the studied cases to then decline again. The first steep increase corresponds to the start of the pseudo-reaction modelled. By contrast, the later decline can be explained by a reduction in CO_2 released and an increased amount of the solvent components in the gas phase. Generally, the CO_2 vapour mole fraction aligns with the pressure increase, exhibiting the highest value for DMC/EC 30/70 vol-%, followed by DMC/EC 50/50 vol-% and the lowest for DMC/EC 70/30 vol-%.

The liquid phase CO_2, on the other hand, does not follow this pattern. The highest liquid mole fraction for CO_2 is observed for DMC/EC 70/30 vol-%, followed by the DMC/EC 50/50 vol-% reference and eventually the DMC/EC 30/70 vol-%. The reason is the higher solubility of CO_2 in DMC over EC. The more linear carbonates present in the mixture, the more CO_2 can dissolve in the liquid phase, thus mitigating the pressure increase. This indicates that the amount of reaction gases and their solubility in the solvent mixture define the pressure progression during a thermal event in Li-ion batteries.

Consequently, considering a gas source mimicking gas-releasing reactions suggests a re-evaluation of our previous understanding; the safety of cyclic carbonates and the perceived risk of linear carbonates are reversed. From these findings, a general rule regarding the choice of

solvents can be deduced: if gas-releasing reactions cannot be avoided, the solvents should be chosen or designed so that the evolving gases have high solubility in them. In our case, we considered CO_2 as degradation gas, which has a higher solubility in linear carbonates than cyclic carbonates. Therefore, from a safety perspective, linear carbonates are favoured. However, this may change if gases with higher solubility in cyclic carbonates are added to the analysis.

CO_2 and the further typical measured degradation gases H_2, CO, and C_2H_4 make up above 90% of measured gases [6,63,64]. For all gases mentioned the solubility is higher in linear than in cyclic carbonates [79,98–101]. Gases like PF_5 and POF_3, from the decomposition of $LiPF_6$, are also found to evolve in the early stages of a thermal event [88,102]. For these, no solubility data is currently available. Thus, their influence on the pressure increase during a thermal event cannot be addressed here. However, since most gases from degradation reactions are shown to be more soluble in linear carbonates and due to the higher reactivity of cyclic carbonates with the negative electrode [103], it is doubtful that a higher concentration of cyclic carbonates will lead to lower pressures and, therefore, safer batteries.

Furthermore, we re-evaluate the liquid-to-void volume percentage during manufacturing at room temperature and how a including a gas source impacts it. In Fig. 5(d), a variation in liquid vol-% (of 70, 80 and 90 vol-%) is shown for a DMC/EC 50/50 vol-% mixture. We assume composition-independent reaction, based on 15 mol-% conversion of EC in a DMC/EC 50/50 vol-% mixture with 70 vol-% liquid volume Compared to previous cases, the assumption of constant vol-% has to be added since an increased liquid volume also increases the molar amount of EC in the system. Below 100 °C, the pressure evolution is almost identical, showing a maximum deviation of below 2%; see ESI. At this point, all cases reach the CID activation pressure of 10 bar. Above 100 °C, the cases with a higher electrolyte filling show a slightly higher pressure than the 70 vol-% reference. However, the difference is less than 5% even for the 90 vol-% case. Due to the minimal differences in pressure increase, all cases reach the venting pressure of 20 bar in a temperature window of 142 °C–144 °C. This additional analysis reinforces our prior conclusions regarding the liquid-to-gas volume ratio. It indicates that the ratio can be safely raised from the previously reported figures of 50 vol-% [9] and 70 vol-% [90], to at least 85 vol-% without significantly increasing safety risks, such as venting of the battery at lower temperatures.

3.3. Discussion on transferability of the results

Pressure evolution during the thermal abuse of Li-ion batteries depends on the evolving gases and their vapour–liquid equilibria with the solvents, i.e., the solubility of corresponding gases. In our current study, we provide important insights into the underlying principles and proposed mitigation strategies. However, since the system studied does not include a full reaction model, here presented mitigation strategies focus on the electrolyte impact. In a real system, additional processes and additives are present, whose quantitative effect needs to be studied in future.

For example, state-of-the-art electrolyte formulations for Li-ion batteries contain several functional additives [104]. These will impact the vapour–liquid equilibria, i.e., the boiling point and gas solubility, in several ways. We consider the boiling points of some pure compounds for a first assessment of the expected impact of such additives. Boiling points higher than the low-boiling linear carbonates, i.e., above 108 °C for DMC or 115 °C for EMC, will potentially lower the pressure of the mixture. The film forming additives vinylene carbonate (VC), $T_{b,VC}$ = 162 °C [105], fluoro ethylene carbonate (FEC), $T_{b,FEC}$ = 212 °C [106], and the flame-retardant additive dimethyl phosphate (DMP), $T_{b,DMP}$ = 171 °C [107], all have higher boiling points than the solvents. Thus, they should decrease the pressure.

In the previous section, we showed that gas solubility has a higher influence on the vapour–liquid equilibrium than the boiling points of the solvents. Future studies that consider evaluating the impact of additives on vapour–liquid equilibria and pressure evolution in Li-ion electrolytes will, thus, require identifying solubility parameters for these additives.

Moreover, the largest uncertainty stems from the unknown impact of the myriad of gas-evolving degradation reactions. Since in our current study we focus on the vapour–liquid equilibrium, we cannot say with certainty how changing the electrolyte composition or the addition of additives will alter the pressure evolution due to altering the reaction pathways of the system. However, it provides evidence of the dramatic influence that degradation reactions can have on cell safety. Our study also serves as a starting point to provide important insights for electrolyte design and to open doors for future research endeavours.

4. Conclusions

Pressure evolution in Li-ion batteries is an essential factor when assessing battery safety at elevated temperatures. In the current work we have introduced a model-based assessment of the thermodynamic effects of electrolyte composition on pressure evolution using a vapour–liquid equilibrium model based on the SAFT-γ Mie group-contribution framework. This has allowed us to investigate the influence of varying the solvent composition, the gas solubility, the conductive salt $LiPF_6$ concentration, and CO_2-evolving reaction on the pressure at phase equilibrium during heating of the cell to 250 °C.

We reveal that a battery optimised for volumetric energy density with low or no gas volume left would suffer severe safety issues. The expanding liquid phase will lead to a dramatic pressure rise even below 100 °C. However, in commercially available cells, there is still room for optimisation. In the absence of degradation reactions, the presently employed liquid volume percentage of 70 to 50 vol-% could possibly be increased to 85 vol-% without elevated safety risk below 200 °C, according to our calculations. This is also shown for systems considering a simplified gassing reaction.

Further, we find that the choice of low-boiling linear carbonates, such as DMC and EMC, is crucial in non-reactive systems. The choice of the higher-boiling EMC over the lower-boiling DMC can decrease the pressure up to 39%, see Fig. 6. When considering different pad gases, a gas with high solubility increases the pressure, up to 20%, see Fig. 6. From this observation, the general rule is that an optimal pad gas should have a low solubility in the solvent mixture and further increase its solubility with increasing temperature. Argon or other noble gases are good examples exhibiting both characteristics. However, as they must be produced with significant effort, nitrogen, which is already used in industrial settings, is an equally good alternative due to its lower solubility than argon.

A comparison of different cell casings leads to the conclusion that almost no solvent boiling would occur in a closed cell. On the other hand, when considering expandable systems, such as pouch cells, evaporation was found to occur to a noticeable extent. This may act as a considerable heat sink in the early phase of self-heating. Comparing an expandable pouch-cell with a rigid cell casing, such as a prismatic cell, showed a 50% higher pressure in the rigid cell casing, see Fig. 6.

Adding $LiPF_6$ as the conductive salt is found to give rise to only a slight 5% deviation, see Fig. 6, in the system pressure compared to the solvent system without added salt, indicating that it is not a significant factor. Based on our current understanding, the $LiPF_6$ concentration can be optimised to maximise performance without compromising safety, as no negative effect on safety has been identified.

Finally, we find that even mild gas-releasing reactions can trigger safety valve opening over the analysed temperature range from 25 to 250 °C. The higher solubility of CO_2 in linear carbonates has a higher and indeed dampening impact on pressure evolution, leading to a up to 20% lower pressure for systems with higher concentrations of linear carbonates (see Fig. 6). This is even despite their low boiling points,

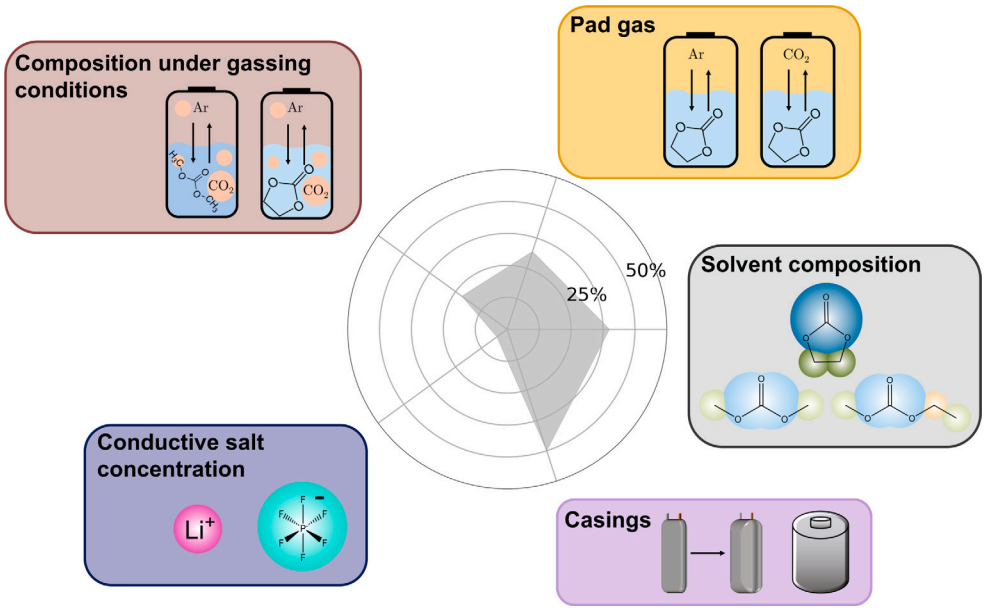

Fig. 6. Comparative figure illustrating the impact of solvent composition, conductive salt, pad gas, casings and solvent composition under gassing conditions on pressure evolution by showing the maximum deviation in each study.

which, in contrast, accelerates the pressure evolution. The solvent system should thus always be chosen so that the solubility of possible gases stemming from degradation reactions is as high as possible. Comparing the solubilities of other common degradation gases in linear and cyclic carbonates showed that most reaction gases are more soluble in linear than in cyclic carbonates.

Future studies may address the open challenge of incorporating a more thorough reaction network to study the interwoven effects of evolving reaction gases caused by elevated temperatures, the resulting pressure increase, and its subsequent effect on the underlying reactions. The current assumption of maintained phase equilibria at all times is only valid for slow heating rates. Future works could address this by moving to a model that incorporates mass and heat transfer limitations. Eventually, this will allow one to obtain a holistic picture of a different batteries based on their electrode and electrolyte chemistries.

CRediT authorship contribution statement

Florian Baakes: Writing – original draft, Visualization, Validation, Software, Methodology, Investigation, Funding acquisition, Conceptualization. **Roger Song:** Software, Investigation, Data curation. **Thomas Bernet:** Writing – review & editing, Conceptualization. **Jorge Valenzuela García de León:** Software, Methodology. **George Jackson:** Writing – review & editing, Conceptualization. **Claire S. Adjiman:** Writing – review & editing, Supervision, Conceptualization. **Amparo Galindo:** Writing – review & editing, Supervision, Conceptualization. **Ulrike Krewer:** Writing – review & editing, Supervision, Funding acquisition, Conceptualization.

Declaration of competing interest

The authors declare that they have no known competing financial interests or personal relationships that could have appeared to influence the work reported in this paper.

Acknowledgements

This work was supported by the German Federal Ministry for Economic Affairs and Climate Action through funding of the project "SimDural — Simulation-based Safety Analysis of an Uncontrolled Thermal Runaway in Aged Battery Cells". (16BZF325C) and the Karlsruhe House of Young Scientist through funding a research stay.

Appendix A. Supplementary data

Supplementary material related to this article can be found online at https://doi.org/10.1016/j.jpowsour.2025.236619.

Data availability

Data presented in the figures of this manuscript are provided in the KITopen repository under https://doi.org/10.35097/6j6r99kgrvjp09hs.

References

[1] P. Sun, R. Bisschop, H. Niu, X. Huang, A review of battery fires in electric vehicles, Fire Technol. 56 (4) (2020) 1361–1410, http://dx.doi.org/10.1007/s10694-019-00944-3.

[2] L.B. Diaz, X. He, Z. Hu, F. Restuccia, M. Marinescu, J.V. Barreras, Y. Patel, G. Offer, G. Rein, Meta-review of fire safety of lithium-ion batteries: Industry challenges and research contributions, J. Electrochem. Soc. 167 (9) (2020) 090559, http://dx.doi.org/10.1149/1945-7111/aba8b9.

[3] F. Baakes, M. Lüthe, M. Gerasimov, V. Laue, F. Röder, P.B. Balbuena, U. Krewer, Unveiling the interaction of reactions and phase transition during thermal abuse of Li-ion batteries, J. Power Sources 522 (2022) http://dx.doi.org/10.1016/j.jpowsour.2021.230881.

[4] J. Kim, A. Mallarapu, D.P. Finegan, S. Santhanagopalan, Modeling cell venting and gas-phase reactions in 18650 lithium-ion batteries during thermal runaway, J. Power Sources 489 (2021) http://dx.doi.org/10.1016/j.jpowsour.2021.229496.

[5] F. Baakes, D. Witt, U. Krewer, Impact of electrolyte impurities and SEI composition on battery safety, Chem. Sci. 14 (2023) 13783–13798, http://dx.doi.org/10.1039/D3SC04186G.

[6] A.W. Golubkov, D. Fuchs, J. Wagner, H. Wiltsche, C. Stangl, G. Fauler, G. Voitic, A. Thaler, V. Hacker, Thermal-runaway experiments on consumer lithium-ion batteries with metal-oxide and olivin-type cathodes, RSC Adv. 4 (7) (2014) 3633–3642, http://dx.doi.org/10.1039/c3ra45748f.

[7] B. Lei, W. Zhao, C. Ziebert, N. Uhlmann, M. Rohde, H.J. Seifert, Experimental analysis of thermal runaway in 18650 cylindrical lithium-ion cells using an accelerating rate calorimeter, Batteries 3 (2) (2017) http://dx.doi.org/10.3390/batteries3020014.

[8] C.Y. Jhu, Y.W. Wang, C.M. Shu, J.C. Chang, H.C. Wu, Thermal explosion hazards on 18650 lithium-ion batteries with a VSP2 adiabatic calorimeter, J. Hazard. Mater. 192 (1) (2011) 99–107, http://dx.doi.org/10.1016/j.jhazmat.2011.04.097.

[9] P.T. Coman, S. Mátéfi-Tempfli, C.T. Veje, R.E. White, Modeling vaporization, gas generation and venting in lithium-ion battery cells with a dimethyl carbonate electrolyte, J. Electrochem. Soc. 164 (9) (2017) A1858–A1865, http://dx.doi.org/10.1149/2.0631709jes.

[10] C.M. Vendra, A.V. Shelke, J.E. Buston, J. Gill, D. Howard, E. Read, A. Abaza, B. Cooper, J.X. Wen, Numerical and experimental characterisation of high energy density 21700 lithium-ion battery fires, Process. Saf. Environ. Prot. 160 (2022) 153–165, http://dx.doi.org/10.1016/j.psep.2022.02.014.

[11] A. Kriston, I. Adanouj, V. Ruiz, A. Pfrang, Quantification and simulation of thermal decomposition reactions of lithium-ion battery materials by simultaneous thermal analysis coupled with gas analysis, J. Power Sources 435 (2019) http://dx.doi.org/10.1016/j.jpowsour.2019.226774.

[12] M. Gerasimov, F.A. Soto, J. Wagner, F. Baakes, N. Guo, F. Ospina-Acevedo, F. Röder, P.B. Balbuena, U. Krewer, Species distribution during solid electrolyte interphase formation on lithium using MD/DFT-parameterized kinetic Monte Carlo simulations, J. Phys. Chem. C 127 (10) (2023) 4872–4886, http://dx.doi.org/10.1021/acs.jpcc.2c05898.

[13] J. Wagner-Henke, D. Kuai, M. Gerasimov, F. Röder, P.B. Balbuena, U. Krewer, Knowledge-driven design of solid-electrolyte interphases on lithium metal via multiscale modelling, Nat. Commun. 14 (1) (2023) 6823, http://dx.doi.org/10.1038/s41467-023-42212-7.

[14] B. Horstmann, J. Shi, R. Amine, M. Werres, X. He, H. Jia, F. Hausen, I. Cekic-Laskovic, S. Wiemers-Meyer, J. Lopez, D. Galvez-Aranda, F. Baakes, D. Bresser, C.C. Su, Y. Xu, W. Xu, P. Jakes, R.A. Eichel, E. Figgemeier, U. Krewer, J.M. Seminario, P.B. Balbuena, C. Wang, S. Passerini, Y. Shao-Horn, M. Winter, K. Amine, R. Kostecki, A. Latz, Strategies towards enabling lithium metal in batteries: Interphases and electrodes, Energy Environ. Sci. 14 (10) (2021) 5289–5314, http://dx.doi.org/10.1039/d1ee00767j.

[15] X. He, D. Bresser, S. Passerini, F. Baakes, U. Krewer, J. Lopez, C.T. Mallia, Y. Shao-Horn, I. Cekic-Laskovic, S. Wiemers-Meyer, F.A. Soto, V. Ponce, J.M. Seminario, P.B. Balbuena, H. Jia, W. Xu, Y. Xu, C. Wang, B. Horstmann, R. Amine, C.C. Su, J. Shi, K. Amine, M. Winter, A. Latz, R. Kostecki, The passivity of lithium electrodes in liquid electrolytes for secondary batteries, Nat. Rev. Mater. 6 (11) (2021) 1036–1052, http://dx.doi.org/10.1038/s41578-021-00345-5.

[16] K. Xu, Nonaqueous liquid electrolytes for lithium-based rechargeable batteries, Chem. Rev. 104 (10) (2004) 4303–4418, http://dx.doi.org/10.1021/cr030203g.

[17] L. Chen, H. Wu, X. Ai, Y. Cao, Z. Chen, Toward wide-temperature electrolyte for lithium–ion batteries, Batter. Energy 1 (2) (2022) 20210006, http://dx.doi.org/10.1002/bte2.20210006.

[18] Y.-K. Liu, C.-Z. Zhao, J. Du, X.-Q. Zhang, A.-B. Chen, Q. Zhang, Research progresses of liquid electrolytes in lithium-ion batteries, Small 19 (8) (2023) 2205315, http://dx.doi.org/10.1002/smll.202205315.

[19] P. Coutsikos, N.S. Kalospiros, D.P. Tassios, Capabilities and limitations of the Wong-Sandler mixing rules, Fluid Phase Equilib. 108 (1–2) (1995) 59–78, http://dx.doi.org/10.1016/0378-3812(94)02675-Q.

[20] G.M. Kontogeorgis, X. Liang, A. Arya, I. Tsivintzelis, Equations of state in three centuries. Are we closer to arriving to a single model for all applications? Chem. Eng. Science: X 7 (2020) http://dx.doi.org/10.1016/j.cesx.2020.100060.

[21] W. Chapman, K. Gubbins, G. Jackson, M. Radosz, SAFT: equation of state solution model for associating fluids, Fluid Phase Equilib. 52 (1989) 31–38, http://dx.doi.org/10.1016/0378-3812(89)80308-5.

[22] W.G. Chapman, K.E. Gubbins, G. Jackson, M. Radosz, New reference equation of state for associating liquids, Ind. Eng. Chem. Res. 29 (8) (1990) 1709–1721, http://dx.doi.org/10.1021/ie00104a021.

[23] M.S. Wertheim, Fluids with highly directional attractive forces. II. Thermodynamic perturbation theory and integral equations, J. Stat. Phys. 35 (2) (1984) http://dx.doi.org/10.1007/BF01017363.

[24] M.S. Wertheim, Fluids with highly directional attractive forces. I. Statistical thermodynamics, J. Stat. Phys. 35 (1984) http://dx.doi.org/10.1007/BF01017362.

[25] M. Wertheim, Fluids with highly directional attractive forces. III. Multiple attraction sites, J. Stat. Phys. 42 (3–4) (1986) 459–476, http://dx.doi.org/10.1007/BF01127721.

[26] M. Wertheim, Fluids with highly directional attractive forces. IV. Equilibrium polymerization, J. Stat. Phys. 42 (3–4) (1986) 477–492, http://dx.doi.org/10.1007/BF01127722.

[27] I.G. Economou, Statistical associating fluid theory: a successful model for the calculation of thermodynamic and phase equilibrium properties of complex fluid mixtures, Ind. Eng. Chem. Res. 41 (5) (2002) 953–962, http://dx.doi.org/10.1021/ie0102201.

[28] C. McCabe, A. Galindo, Applied Thermodynamics of Fluids, The Royal Society of Chemistry, 2010, Ch. 8: SAFT associating fluids and fluid mixture. http://dx.doi.org/10.1039/9781849730983-00215.

[29] J. Gross, G. Sadowski, Application of perturbation theory to a hard-chain reference fluid: an equation of state for square-well chains, Fluid Phase Equilib. 168 (2000) 183–199, http://dx.doi.org/10.1016/S0378-3812(00)00302-2.

[30] J. Gross, G. Sadowski, Perturbed-chain SAFT: An equation of state based on a perturbation theory for chain molecules, Ind. Eng. Chem. Res. 40 (4) (2001) 1244–1260, http://dx.doi.org/10.1021/ie0003887.

[31] F.J. Blas, L.F. Vega, Thermodynamic behaviour of homonuclear and heteronuclear Lennard-Jones chains with association sites from simulation and theory, Mol. Phys. 92 (1) (1997) 135–150, http://dx.doi.org/10.1080/002689797170707.

[32] A. Gil-Villegas, A. Galindo, P.J. Whitehead, S.J. Mills, G. Jackson, A.N. Burgess, Statistical associating fluid theory for chain molecules with attractive potentials of variable range, J. Chem. Phys. 106 (10) (1997) 4168–4186, http://dx.doi.org/10.1063/1.473101.

[33] A. Lymperiadis, C.S. Adjiman, G. Jackson, A. Galindo, A generalisation of the SAFT-γ group contribution method for groups comprising multiple spherical segments, Fluid Phase Equilib. 274 (1–2) (2008) 85–104, http://dx.doi.org/10.1016/j.fluid.2008.08.005.

[34] Y. Peng, K.D. Goff, M.C. dos Ramos, C. McCabe, Developing a predictive group-contribution-based SAFT-VR equation of state, Fluid Phase Equilib. 277 (2) (2009) 131–144, http://dx.doi.org/10.1016/j.fluid.2008.11.008.

[35] T. Lafitte, A. Apostolakou, C. Avendaño, A. Galindo, C.S. Adjiman, E.A. Müller, G. Jackson, Accurate statistical associating fluid theory for chain molecules formed from Mie segments, J. Chem. Phys. 139 (15) (2013) 154504, http://dx.doi.org/10.1063/1.4819786.

[36] V. Papaioannou, T. Lafitte, C. Avendaño, C.S. Adjiman, G. Jackson, E.A. Müller, A. Galindo, Group contribution methodology based on the statistical associating fluid theory for heteronuclear molecules formed from Mie segments, J. Chem. Phys. 140 (5) (2014) 054107, http://dx.doi.org/10.1063/1.4851455.

[37] S. Dufal, V. Papaioannou, M. Sadeqzadeh, T. Pogiatzis, A. Chremos, C.S. Adjiman, G. Jackson, A. Galindo, Prediction of thermodynamic properties and phase behavior of fluids and mixtures with the SAFT-γ Mie group-contribution equation of state, J. Chem. Eng. Data 59 (10) (2014) 3272–3288, http://dx.doi.org/10.1021/je500248h.

[38] J.M. Schreckenberg, S. Dufal, A.J. Haslam, C.S. Adjiman, G. Jackson, A. Galindo, Modelling of the thermodynamic and solvation properties of electrolyte solutions with the statistical associating fluid theory for potentials of variable range, Mol. Phys. 112 (17) (2014) 2339–2364, http://dx.doi.org/10.1080/00268976.2014.910316.

[39] D.K. Eriksen, G. Lazarou, A. Galindo, G. Jackson, C.S. Adjiman, A.J. Haslam, Development of intermolecular potential models for electrolyte solutions using an electrolyte SAFT-VR Mie equation of state, Mol. Phys. 114 (18) (2016) 2724–2749, http://dx.doi.org/10.1080/00268976.2016.1236221.

[40] A.J. Haslam, A. González-Pérez, S. Di Lecce, S.H. Khalit, F.A. Perdomo, S. Kournopoulos, M. Kohns, T. Lindeboom, M. Wehbe, S. Febra, G. Jackson, C.S. Adjiman, A. Galindo, Expanding the applications of the SAFT-γMie group-contribution equation of state: Prediction of thermodynamic properties and phase behavior of mixtures, J. Chem. Eng. Data 65 (12) (2020) 5862–5890, http://dx.doi.org/10.1021/acs.jced.0c00746.

[41] S.A. Krachkovskiy, J.D. Bazak, S. Fraser, I.C. Halalay, G.R. Goward, Determination of mass transfer parameters and ionic association of $LiPF_6$: Organic carbonates solutions, J. Electrochem. Soc. 164 (4) (2017) A912–A916, http://dx.doi.org/10.1149/2.1531704jes.

[42] M.A. Rivas, S.M. Pereira, T.P. Iglesias, Relative permittivity of the mixtures (dimethyl or diethyl carbonate) + n-nonane from T=288.15 K to T=308.15 K, J. Chem. Thermodyn. 34 (11) (2002) 1897–1907, http://dx.doi.org/10.1016/S0021-9614(02)00260-4.

[43] C.G. Malmberg, A.A. Maryott, Dielectric constant of water from 0°C to 100°C, J. Res. Natl. Bur. Stand. 56 (I) (1956).

[44] R. Payne, I.E. Theodorou, Dielectric properties and relaxation in ethylene carbonate and propylene carbonate, J. Phys. Chem. 76 (20) (1972) 2892–2900, http://dx.doi.org/10.1021/j100664a019.

[45] Z. Feng, K. Higa, K.S. Han, V. Srinivasan, Evaluating transport properties and ionic dissociation of $LiPF_6$ in concentrated electrolyte, J. Electrochem. Soc. 164 (12) (2017) A2434–A2440, http://dx.doi.org/10.1149/2.0941712jes.

[46] Y. Marcus, G. Hefter, Ion pairing, Chem. Rev. 106 (11) (2006) 4585–4621, http://dx.doi.org/10.1021/cr040087x.

[47] B. Koo, H. Lee, S. Hwang, H. Lee, Ionic conduction and speciation in $LiPF_6$ and $LiBF_4$ dimethyl sulfoxide electrolytes: Comparison with propylene carbonate electrolytes, J. Phys. Chem. C (2022) 5676–5682, http://dx.doi.org/10.1021/acs.jpcc.2c08977.

[48] H. Krienke, J. Barthel, MSA models of ion association in electrolyte solutions, Z. Phys. Chem. 204 (1998) 71–83, http://dx.doi.org/10.1524/zpch.1998.204.Part_1_2.071.

[49] S. Dufal, T. Lafitte, A.J. Haslam, A. Galindo, G.N. Clark, C. Vega, G. Jackson, The A in SAFT: Developing the contribution of association to the Helmholtz free energy within a Wertheim TPT1 treatment of generic Mie fluids, Mol. Phys. 113 (9–10) (2015) 948–984, http://dx.doi.org/10.1080/00268976.2015.1029027.

[50] G. Lazarou, Development of the SAFT-γ Mie Equation of State for Predicting the Thermodynamic Behaviour of Strong and Weak Electrolyte Solutions (Ph.D. thesis), Imperial College London, London, 2017, http://dx.doi.org/10.25560/60588.

[51] M. Born, Volumen und Hydratationswärme der Ionen, Z. Für Phys. 1 (1) (1920) 45–48, http://dx.doi.org/10.1007/BF01881023.

[52] L. Blum, Solution of a model for the solvent - electrolyte interactions in the mean spherical approximation, J. Chem. Phys. 61 (5) (1974) 2129–2133, http://dx.doi.org/10.1063/1.1682224.

[53] L. Blum, Mean spherical model for asymmetric electrolytes, Mol. Phys. 30 (5) (1975) 1529–1535, http://dx.doi.org/10.1080/00268977500103051.

[54] O. Borodin, G.D. Smith, Quantum chemistry and molecular dynamics simulation study of dimethyl carbonate: Ethylene carbonate electrolytes doped with $LiPF_6$, J. Phys. Chem. B 113 (6) (2009) 1763–1776, http://dx.doi.org/10.1021/jp809614h.

[55] O. Borodin, M. Olguin, P. Ganesh, P.R. Kent, J.L. Allen, W.A. Henderson, Competitive lithium solvation of linear and cyclic carbonates from quantum chemistry, Phys. Chem. Chem. Phys. 18 (1) (2016) 164–175, http://dx.doi.org/10.1039/c5cp05121e.

[56] K. Hayamizu, Temperature dependence of self-diffusion coefficients of ions and solvents in ethylene carbonate, propylene carbonate, and diethyl carbonate single solutions and ethylene carbonate + diethyl carbonate binary solutions of $LiPF_6$ studied by NMR, J. Chem. Eng. Data 57 (7) (2012) 2012–2017, http://dx.doi.org/10.1021/je3003089.

[57] J. Self, N.T. Hahn, K.A. Persson, Solvation effects on the Dielectric constant of 1 M $LiPF_6$ in ethylene carbonate:ethyl methyl carbonate 3:7, Energy Environ. Mater. (2023) http://dx.doi.org/10.1002/eem2.12494.

[58] T. Kawamura, S. Okada, J.i. Yamaki, Decomposition reaction of $LiPF_6$-based electrolytes for lithium ion cells, J. Power Sources 156 (2) (2006) 547–554, http://dx.doi.org/10.1016/j.jpowsour.2005.05.084.

[59] G. Das, S. Hlushak, M.C. dos Ramos, C. Mccabe, Predicting the thermodynamic properties and dielectric behavior of electrolyte solutions using the SAFT-VR+DE equation of state, AIChE J. 61 (9) (2015) 3053–3072, http://dx.doi.org/10.1002/aic.14909.

[60] N. Novak, G.M. Kontogeorgis, M. Castier, I.G. Economou, Extension of the eSAFT-VR Mie equation of state from aqueous to non-aqueous electrolyte solutions, Fluid Phase Equilib. 565 (2023) http://dx.doi.org/10.1016/j.fluid.2022.113618.

[61] M.D. Olsen, G.M. Kontogeorgis, X. Liang, N. von Solms, Comparison of models for the relative static permittivity with the e-CPA equation of state, Fluid Phase Equilib. 565 (2023) http://dx.doi.org/10.1016/j.fluid.2022.113632.

[62] The MathWorks Inc., MATLAB version: 23.2.0 (R2023b), The MathWorks Inc., Natick, Massachusetts, United States, 2023, URL https://www.mathworks.com.

[63] L. Yuan, T. Dubaniewicz, I. Zlochower, R. Thomas, N. Rayyan, Experimental study on thermal runaway and vented gases of lithium-ion cells, Process. Saf. Environ. Prot. 144 (2020) 186–192, http://dx.doi.org/10.1016/j.psep.2020.07.028.

[64] S. Koch, A. Fill, K.P. Birke, Comprehensive gas analysis on large scale automotive lithium-ion cells in thermal runaway, J. Power Sources 398 (2018) 106–112, http://dx.doi.org/10.1016/j.jpowsour.2018.07.051.

[65] J.S. Rowlinson, F.L. Swinton, Liquid and Liquid Mixtures, third ed., Butterworth & Co Ltd, London, 1982.

[66] L. Chen, R.J. Zhu, Y. Fang, P.F. Yuan, L.Q. Cao, Y.L. Tian, Vapor-liquid equilibrium data for carbon dioxide+dimethyl carbonate binary system, Wuli Huaxue Xuebao/ Acta Phys. - Chim. Sin. 29 (1) (2013) 11–16, http://dx.doi.org/10.3866/PKU.WHXB201210262.

[67] M.A. Saleh, S. Akhtar, M.S. Ahmed, M.H. Uddin, Density, excess molar volume, viscosity and thermodynamic activation of viscous flow of water + ethylene carbonate, Phys. Chem. Liq. 43 (4) (2005) 367–377, http://dx.doi.org/10.1080/00319100500130194.

[68] V.D. Kiselev, A.V. Bolotov, P-V-T parameters of propylene carbonate and cis-,trans-decahydronaphthalene in temperature and pressure ranges of 20–50°C and 1–1000 bar, Russ. J. Phys. Chem. A 84 (4) (2010) 593–597, http://dx.doi.org/10.1134/S0036024410040138.

[69] S.A. Kozlova, V.N. Emel'yanenko, M. Georgieva, S.P. Verevkin, Y. Chernyak, B. Schäffner, A. Börner, Vapour pressure and enthalpy of vaporization of aliphatic dialkyl carbonates, J. Chem. Thermodyn. 40 (7) (2008) 1136–1140, http://dx.doi.org/10.1016/j.jct.2008.02.012.

[70] W. Steele, R. Chirico, S. Knipmeyer, A. Nguyen, N. Smith, Thermodynamic properties and ideal-gas enthalpies of formation for dicyclohexyl sulfide, diethylenetriamine, di-n-octyl sulfide, dimethyl carbonate, piperazine, hexachloroprop-1-ene, tetrakis (dimethylamino) ethylene, N, N '-bis-(2-hydroxyethyl) ethylenediamine, and 1, 2, 4-triazolo [1, 5-a] pyrimidine, J. Chem. Eng. Data 42 (6) (1997) 1037–1052, http://dx.doi.org/10.1021/je9700986.

[71] F. Stehmann, P. Prziwara, C. Bradtmöller, M. Schoenitz, S. Scholl, Adsorption equilibria of dimethyl carbonate and ethyl methyl carbonate onto activated carbon, Chemie-Ingenieur-Tech. 88 (3) (2016) 327–335, http://dx.doi.org/10.1002/cite.201500130.

[72] V. Pokorný, V. Štejfa, M. Fulem, C. Červinka, K. Růžička, Vapor pressures and thermophysical properties of dimethyl carbonate, diethyl carbonate, and dipropyl carbonate, J. Chem. Eng. Data 62 (10) (2017) 3206–3215, http://dx.doi.org/10.1021/acs.jced.7b00295.

[73] S.P. Verevkin, A.V. Toktonov, Y. Chernyak, B. Schäffner, A. Börner, Vapour pressure and enthalpy of vaporization of cyclic alkylene carbonates, Fluid Phase Equilib. 268 (1–2) (2008) 1–6, http://dx.doi.org/10.1016/j.fluid.2008.03.013.

[74] C. Hong, R. Wakslak, H. Finston, V. Fried, Some thermodynamic properties of systems containing propylene carbonate and ethylene carbonate, J. Chem. Eng. Data 27 (2) (1982) 146–148, http://dx.doi.org/10.1021/je00028a012.

[75] X. Zhang, J. Zuo, C. Jian, Experimental isobaric vapor-liquid equilibrium for binary systems of ethyl methyl carbonate + methanol, + ethanol, + dimethyl carbonate, or + diethyl carbonate at 101.3 kPa, J. Chem. Eng. Data 55 (11) (2010) 4896–4902, http://dx.doi.org/10.1021/je100494z.

[76] R. Naejus, D. Lemordant, R. Coudert, P. Willmann, Excess thermodynamic properties of binary mixtures containing linear or cyclic carbonates as solvents at the temperatures 298.15 K and 315.15 K, J. Chem. Thermodyn. 29 (1997) 15031515, http://dx.doi.org/10.1006/jcht.1997.0260.

[77] M. Anouti, Y.R. Dougassa, C. Tessier, L. El Ouatani, J. Jacquemin, Low pressure carbon dioxide solubility in pure electrolyte solvents for lithium-ion batteries as a function of temperature. Measurement and prediction, J. Chem. Thermodyn. 50 (2012) 71–79, http://dx.doi.org/10.1016/j.jct.2012.01.027.

[78] F. Blanchard, B. Carré, F. Bonhomme, P. Biensan, D. Lemordant, Solubility of carbon dioxide in alkylcarbonates and lactones, Can. J. Chem. 81 (5) (2003) 385–391, http://dx.doi.org/10.1139/v03-069.

[79] E.M. Terrado, J.I. Pardo, J.S. Urieta, A.M. Mainar, Solubilities of nonpolar gases in dimethyl carbonate and diethyl carbonate, J. Chem. Eng. Data 50 (2) (2005) 512–516, http://dx.doi.org/10.1021/je0496894.

[80] N. Xin, Y. Sun, C.J. Radke, J.M. Prausnitz, Osmotic and activity coefficients for five lithium salts in three non–aqueous solvents, J. Chem. Thermodyn. 132 (2019) 83–92, http://dx.doi.org/10.1016/j.jct.2018.12.016.

[81] H. Lee, S. Hwang, M. Kim, K. Kwak, J. Lee, Y.K. Han, H. Lee, Why does dimethyl carbonate dissociate lithium salt better than other linear carbonates? Critical role of polar conformers, J. Phys. Chem. Lett. 11 (24) (2020) 10382–10387, http://dx.doi.org/10.1021/acs.jpclett.0c03235.

[82] Y.R. Dougassa, C. Tessier, L. El Ouatani, M. Anouti, J. Jacquemin, Low pressure carbon dioxide solubility in lithium-ion batteries based electrolytes as a function of temperature. Measurement and prediction, J. Chem. Thermodyn. 61 (2013) 32–44, http://dx.doi.org/10.1016/j.jct.2012.12.025.

[83] Y.R. Dougassa, J. Jacquemin, L. El Ouatani, C. Tessier, M. Anouti, Viscosity and carbon dioxide solubility for $LiPF_6$, LiTFSI, and LiFAP in alkyl carbonates: lithium salt nature and concentration effect, J. Phys. Chem. B 118 (14) (2014) 3973–3980, http://dx.doi.org/10.1021/jp500063c.

[84] Process Systems Enterprise, gPROMS Process Academic Teaching, 1997–2023.

[85] A. Mejía, E.A. Muller, G. Chaparro Maldonado, SGTPy: A Python code for calculating the interfacial properties of fluids based on the square gradient theory using the SAFT-VR Mie equation of state, J. Chem. Inf. Model. 61 (3) (2021) 1244–1250, http://dx.doi.org/10.1021/acs.jcim.0c01324.

[86] P.J. Walker, H.-W. Yew, A. Riedemann, Clapeyron. jl: An extensible, open-source fluid thermodynamics toolkit, Ind. Eng. Chem. Res. 61 (20) (2022) 7130–7153, http://dx.doi.org/10.1021/acs.iecr.2c00326.

[87] S.S. Lee, T.H. Kim, S.J. Hu, W.W. Cai, J.A. Abell, Joining technologies for automotive lithium-ion battery manufacturing: A review, in: International Manufacturing Science and Engineering Conference, vol. 49460, 2010, pp. 541–549, http://dx.doi.org/10.1115/MSEC2010-34168.

[88] L. Bläubaum, P. Röse, F. Baakes, U. Krewer, Impact of Lithium-Ion Battery Separators on Gas Evolution during Temperature Abuse, Batter. & Supercaps (2024) e202300534, http://dx.doi.org/10.1002/batt.202300534.

[89] renata batteries, 36_M_ICP622540PMT, renata batteries, Itlingen, 2019.

[90] C. Kupper, W.G. Bessler, Multi-scale thermo-electrochemical modeling of performance and aging of a $LiFePO_4$ /graphite lithium-ion cell, J. Electrochem. Soc. 164 (2) (2017) A304–A320, http://dx.doi.org/10.1149/2.0761702jes.

[91] W. Li, K.R. Crompton, C. Hacker, J.K. Ostanek, Comparison of current interrupt device and vent design for 18650 format lithium-ion battery caps, J. Energy Storage 32 (2020) http://dx.doi.org/10.1016/j.est.2020.101890.

[92] O. De la Iglesia, A.M. Mainar, J.I. Pardo, J.S. Urieta, Solubilities of nonpolar gases in triethylene glycol dimethyl ether, tetraethylene glycol dimethyl ether, dimethyl carbonate, and diethyl carbonate at 298.15 K and 101.33 kPa partial pressure of gas, J. Chem. Eng. Data 48 (3) (2003) 657–661, http://dx.doi.org/10.1021/je020199q.

[93] F.J. Günter, J. Keilhofer, C. Rauch, S. Rössler, M. Schulz, W. Braunwarth, R. Gilles, R. Daub, G. Reinhart, Influence of pressure and temperature on the electrolyte filling of lithium-ion cells: Experiment, model and method, J. Power Sources 517 (2022) 230668, http://dx.doi.org/10.1016/j.jpowsour.2021.230668.

[94] D. Juarez-Robles, S. Azam, J.A. Jeevarajan, P.P. Mukherjee, Degradation-safety analytics in lithium-ion cells and modules: Part III. Aging and safety of pouch format cells, J. Electrochem. Soc. 168 (11) (2021) 110501, http://dx.doi.org/10.1149/1945-7111/ac30af.

[95] G. Åvall, J. Wallenstein, G. Cheng, K.L. Gering, P. Johansson, D.P. Abraham, Highly concentrated electrolytes: electrochemical and physicochemical characteristics of LiPF6 in propylene carbonate solutions, J. Electrochem. Soc. 168 (5) (2021) 050521, http://dx.doi.org/10.1149/1945-7111/abfdc3.

[96] J. Wang, Y. Yamada, K. Sodeyama, C.H. Chiang, Y. Tateyama, A. Yamada, Superconcentrated electrolytes for a high-voltage lithium-ion battery, Nat. Commun. 7 (1) (2016) 1–9, http://dx.doi.org/10.1038/ncomms12032.

[97] F.A. Mier, S.M. Hill, J. Lamb, M.J. Hargather, Non-invasive internal pressure measurement of 18650 format lithium-ion batteries during thermal runaway, J. Energy Storage 51 (2022) http://dx.doi.org/10.1016/j.est.2022.104322.

[98] M.S. Shaharun, H. Mukhtar, B.K. Dutta, Solubility of carbon monoxide and hydrogen in propylene carbonate and thermomorphic multicomponent hydroformylation solvent, Chem. Eng. Sci. 63 (11) (2008) 3024–3035, http://dx.doi.org/10.1016/j.ces.2008.02.035.

[99] N. Li, P. Ma, S. Xia, Determination of solubility of carbon monoxide in methanol-dimethyl carbonate under high pressure, Shiyou Huagong 34 (1) (2005) 60–64.

[100] A. Behr, D. Obst, C. Schulte, Kinetik der isomerisierenden Hydroformylierung von trans-4-Octen, Chem. Ing. Tech. 76 (7) (2004) 904–910, http://dx.doi.org/10.1002/cite.200400069.

[101] O. Rivas, J. Prausnitz, Sweetening of sour natural gases by mixed-solvent absorption: solubilities of ethane, carbon dioxide, and hydrogen sulfide in mixtures of physical and chemical solvents, AIChE J. 25 (6) (1979) 975–984, http://dx.doi.org/10.1002/aic.690250608.

[102] S. Solchenbach, M. Metzger, M. Egawa, H. Beyer, H.A. Gasteiger, Quantification of PF_5 and POF_3 from side reactions of $LiPF_6$ in lithium-ion batteries, J. Electrochem. Soc. 165 (13) (2018) A3022–A3028, http://dx.doi.org/10.1149/2.0481813jes.

[103] S.E. Sloop, J.B. Kerr, K. Kinoshita, The role of Li-ion battery electrolyte reactivity in performance decline and self-discharge, J. Power Sources 119 (2003) 330–337, http://dx.doi.org/10.1016/S0378-7753(03)00149-6.

[104] J. Kalhoff, G.G. Eshetu, D. Bresser, S. Passerini, Safer electrolytes for lithium-ion batteries: state of the art and perspectives, ChemSusChem 8 (13) (2015) 2154–2175, http://dx.doi.org/10.1002/cssc.201500284.

[105] Sigma Aldrich, Product specification: Vinylene Carbonate, 2024, https://Www.Sigmaaldrich.Com/GB/En/Product/Aldrich/809977.

[106] Sigma Aldrich, Product specification: Fluoroethylene carbonate, 2024, https://Www.Sigmaaldrich.Com/GB/En/Product/Aldrich/757349.

[107] Institut für Arbeitsschutz der Deutschen Gesetzlichen Unfallversicherung, GESTIS - Stoffdatenbank, 2020.